Geological Society of America
Special Paper 296
1995

Porosity, permeability, and basalt metamorphism

Craig E. Manning
Department of Earth and Space Sciences, University of California, Los Angeles, California 90024-1567
Dennis K. Bird
Department of Geology, Stanford University, Stanford, California 94305

ABSTRACT

The effects of primary porosity on fluid flow during contact metamorphism were studied in basalts from central East Greenland. The gabbroic Skaergaard magma intruded interbedded massive and aa basalts with mean macroscopic primary porosities of 4% and 11%, respectively. Heat transport from the cooling gabbros led to three metamorphic mineral zones within 1 km of the contact: the actinolite + chlorite zone beyond 250 m, where the mineral assemblage records peak temperatures (T) of ≤550 °C; the pyroxene zone (T = 700–850 °C); and the olivine zone, within 10 m (T > 850 °C). In the actinolite + chlorite zone, aa clasts record more extensive mineralogic alteration of igneous minerals than do massive samples. Extents of prograde recrystallization in the olivine and pyroxene zones are 100% in both flow morphologies, but modal volumes of retrograde minerals in the pyroxene and olivine zones are higher in aa units. Extents of prograde reactions do not correlate with primary porosity because they were solid-solid reactions that occurred at high temperatures, whereas retrograde alteration involved low-temperature hydration reactions in which the availability of H_2O as a reactant, as controlled by porosity, probably influenced reaction extent. In the pyroxene zone, where mineralogic and textural evidence suggests oxygen isotope exchange equilibrium, whole-rock $\delta^{18}O$ compositions are 1.7‰ to 3.0‰ and are similar or lower in aa units than in massive units at any given distance from the contact. The isotopic ratios suggest average time-integrated fluid fluxes of 3.6 and 4.0 × 10^3 mol cm^{-2} in massive and aa units, respectively, if fluid infiltration occurred during prograde metamorphism. Similar values were computed assuming that part of the isotopic exchange was retrograde. These differences imply that time-averaged matrix permeability was ~10% higher in aa flow breccias.

INTRODUCTION

Porosity and permeability vary widely in basalts (e.g., Stearns, 1942; Davis, 1969; Wood and Fernandez, 1988). Heterogeneities in these properties are controlled in part by primary morphological contrasts between and within basalt lava flows. For example, in Hawaii, the Columbia Plateau, and the Deccan Traps, high porosities and permeabilities are found in aa flows, vesiculated flow tops, and rubbly flow bases, whereas low porosities and permeabilities characterize sills and massive lavas (e.g., Stearns and Vaksvik, 1935; Takasaki and Valencio, 1969; Atlantic-Richfield Hanford Company, 1976; Uhl and Joshi, 1986; Hunt et al., 1988; Lindholm and Vacaro, 1988; Drost et al., 1990; Gonthier, 1990; Ingrebritsen and Scholl, 1993). Because fluids in these pore spaces transport heat and matter at high pressures and temperatures, variations in primary hydrologic properties may lead to important contrasts in fluid-rock interaction during basalt metamorphism (e.g., Nabalek et al., 1984; Ferry, 1988; Chamberlain and Conrad, 1991).

Manning, C. E., and Bird, D. K., 1995, Porosity, permeability, and basalt metamorphism, *in* Schiffman, P., and Day, H. W., eds., Low-Grade Metamorphism of Mafic Rocks: Boulder, Colorado, Geological Society of America Special Paper 296.

In this chapter we explore the influence of primary porosity on metamorphic fluid flow in basalts. We studied interbedded brecciated and massive basaltic lavas from central East Greenland: these units define a hydrostratigraphy of alternating high and low porosity that was metamorphosed during the emplacement and cooling of the Skaergaard intrusion. By comparing metamorphic mineral compositions, extents of reactions, and oxygen isotope ratios in the two lava morphologies, we establish links between primary porosity, permeability, and basalt metamorphism. Our results suggest that accounting for primary porosity variations affords a better understanding of basalt-fluid interaction in contact aureoles, regional metamorphic terranes, and hydrothermal systems of the mid-ocean ridges and elsewhere.

GEOLOGIC AND HYDROLOGIC SETTINGS

Geologic background

The basaltic lavas, breccias, and tuffs of central East Greenland were extruded in the early Tertiary during the inception of rifting of the North Atlantic ocean basin (Nielsen, 1978; Brooks, 1980; Nielsen et al., 1981; Brooks and Nielsen, 1982a, 1982b; Larsen and Watt, 1985; Larsen et al., 1989). The basalts unconformably overlie Precambrian gneissic amphibolites and Upper Cretaceous to Paleocene sedimentary rocks (Fig. 1). The Vandfaldsdalen Formation comprises the lowermost 500 m of the basalts in Figure 1 and can be divided into two parts: the lower Vandfaldsdalen Formation, containing both subaqueous and subaerial extrusive rocks; and the upper Vandfaldsdalen Formation, composed of subaerial volcaniclastic breccias, aa flows, and pahoehoe flows (Soper et al., 1976a, 1976b; Nielsen et al., 1981; Manning and Bird, 1991).

After extrusion and burial to a depth of 6–7 km (Brooks and Nielsen, 1982b), the basalts were metamorphosed by intrusions of mafic dikes, sills, and plutons. The tholeiitic Skaergaard intrusion contributed most of the thermal energy that caused metamorphism in the area. The magma chamber inflated rapidly to its maximum volume of ~180 km^3 of magma in ~1000 yr, completely crystallized in ~130,000 yr, and cooled to near-ambient conditions in ~500,000 yr (Norton and Taylor, 1979; Norton et al., 1984). During cooling of the gabbros, heat transport and ground-water circulation caused oxygen isotope and mineralogic alteration of the gabbros and country rocks (Wager and Deer, 1939; Wager and Brown, 1967; Myers, 1978; Taylor and Forester, 1979; Norton and Taylor, 1979; Norton et al., 1984; Bird et al., 1985, 1986, 1988; Manning and Bird, 1986, 1990, 1991; Manning et al., 1993).

We studied the eastern margin of the Skaergaard intrusion (Fig. 1), where the gabbros are in contact with basaltic flows and volcaniclastic breccias of the upper Vandfaldsdalen Formation (Figs. 2 and 3). As summarized by Manning and Bird (1991), the 10 extrusive units of this study area (uvl–uv10) represent the lower 70% of the upper Vandfaldsdalen Formation. Unit uvl is a polymict volcaniclastic breccia with a matrix of fine-grained basaltic detritus. Units uv2–uv10 compose a sequence of fine-grained vesicular flows (uv3, 5, 7, 9) interbedded with monomict flow breccias with massive centers that we interpret as aa flows (uv2, 4, 6, 8, 10). Before emplacement of the Skaergaard magma, the rocks of the study area were intruded by a diabase sill and three north-south diabase dikes (Fig. 2). The Skaergaard intrusion and a related set of sills and northeast-trending dikes were emplaced at ~55 Ma (Brooks and Gleadow, 1979; Brooks and Nielsen, 1982a; Hirschmann, 1992). Subsequent deformation associated with rifting and the emplacement of east-west dikes (Fig. 1) tilted the rocks 10°–20° to the south.

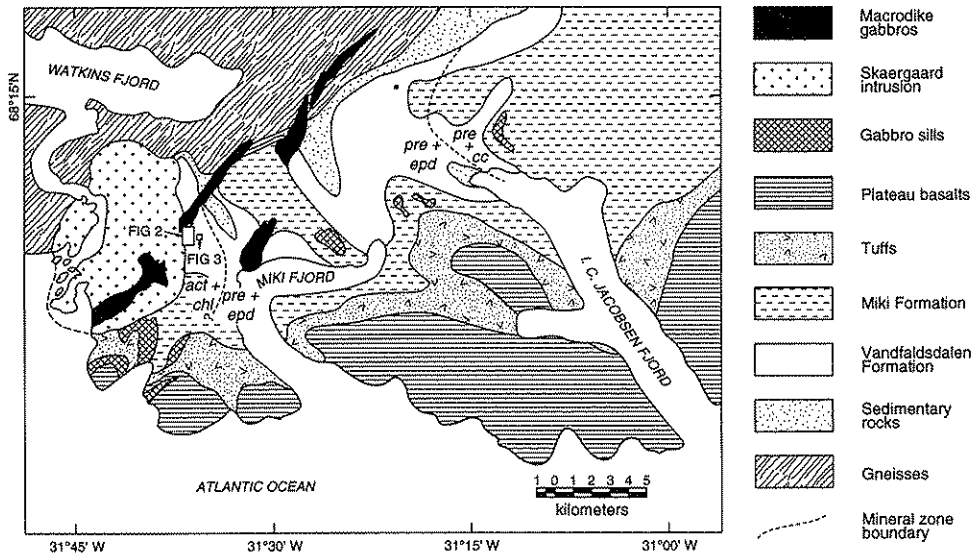

Figure 1. Geologic map of the region east of the Skaergaard intrusion. Mineral zone abbreviations: pre + cc, prehnite + calcite zone; pre + epd, prehnite + epidote zone; act + chl, actinolite + chlorite zone.

Hydrologic background

Quantifying hydrologic properties associated with metamorphism is difficult. Laboratory measurements can characterize porosity and permeability on a hand-sample scale (e.g., Norton and Knapp, 1977; Brace, 1980), but there are two problems in using such measurements in hydrologic studies of metamorphism. First, larger scale features such as faults and fractures may control permeability during metamorphism. Second, metamorphic processes modify the pore network through which fluids migrate, making it difficult to measure porosity and permeability and to assess their changes with time for a given metamorphic event (e.g., Moskowitz and Norton, 1977; Norton, 1984, 1988, 1990; Walder and Nur, 1984; Titley, 1990).

To address these issues we developed a framework for interpreting the evolution of porosity during metamorphism. Detailed mapping and measurement of pore structures allows determination of the macroscopic time-integrated, or cumulative, porosity. Using this variable, Manning and Bird (1991) outlined the hydrologic evolution of the study area. Five pore morphologies occur east of the intrusive contact, including pri-

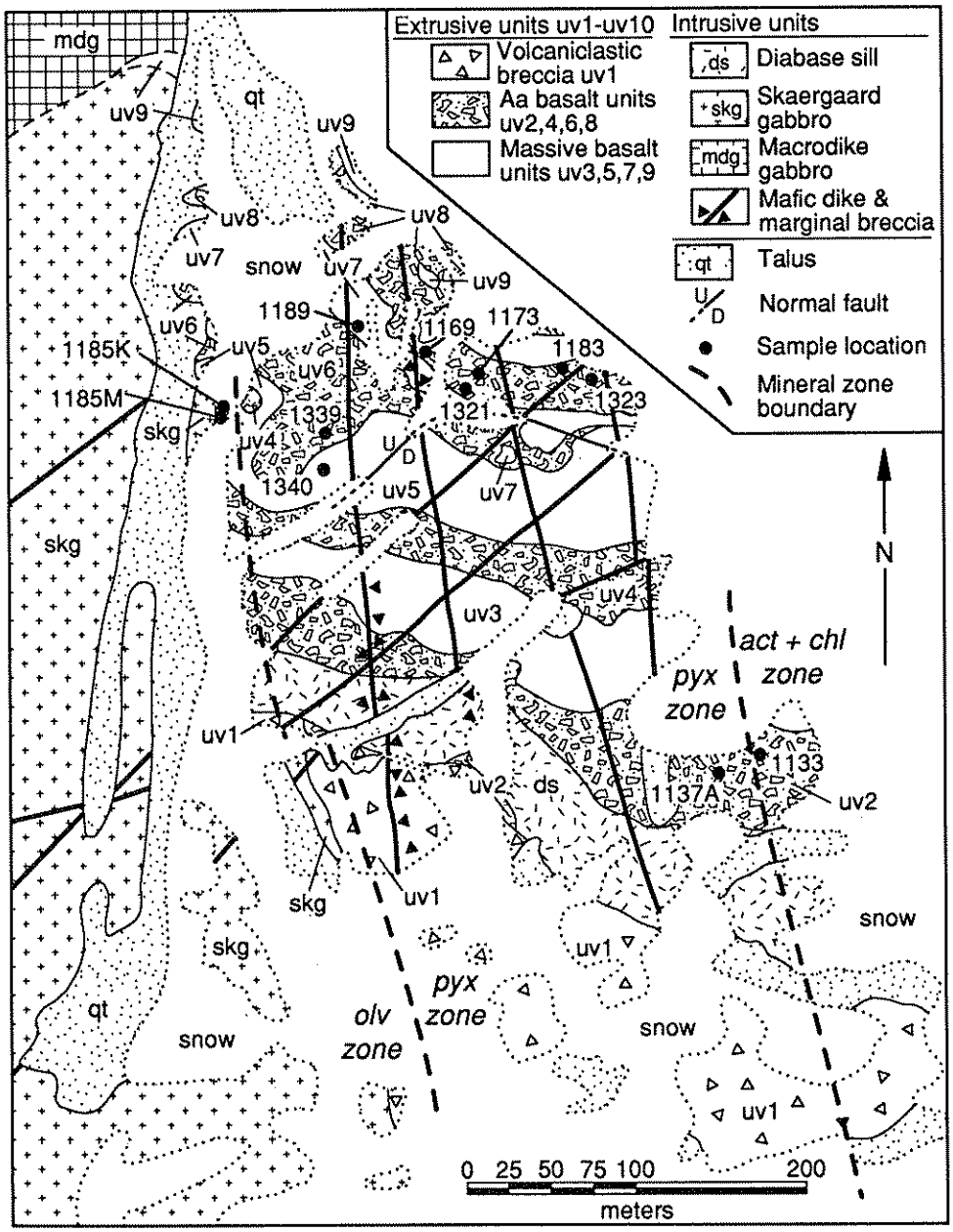

Figure 2. Geologic map of the study area. See Figure 1 for location. Modal volumes and oxygen isotope ratios were determined for samples shown by filled circles. Mineral zone abbreviations: olv, olivine zone; pyx, pyroxene zone; act + chl, actinolite + chlorite zone.

mary pores and four types of secondary pore structures. All cumulative porosities for secondary pores are lower than those of primary pores by at least two orders of magnitude. We therefore suggested that although permeability was enhanced during metamorphism by the development of secondary fractures and breccias, the largest volume of fluid resided in primary pores at any given time. Except in a narrow zone within 150 m of the contact where the pore network displays strong vertical connectivity, the dominant geometry of fluid flow was subhorizontal and toward the pluton (Norton and Taylor, 1979; Manning and Bird, 1991). Thus the hydrologic character of the stratigraphy probably influenced strongly the evolution of fluid flow and metamorphism.

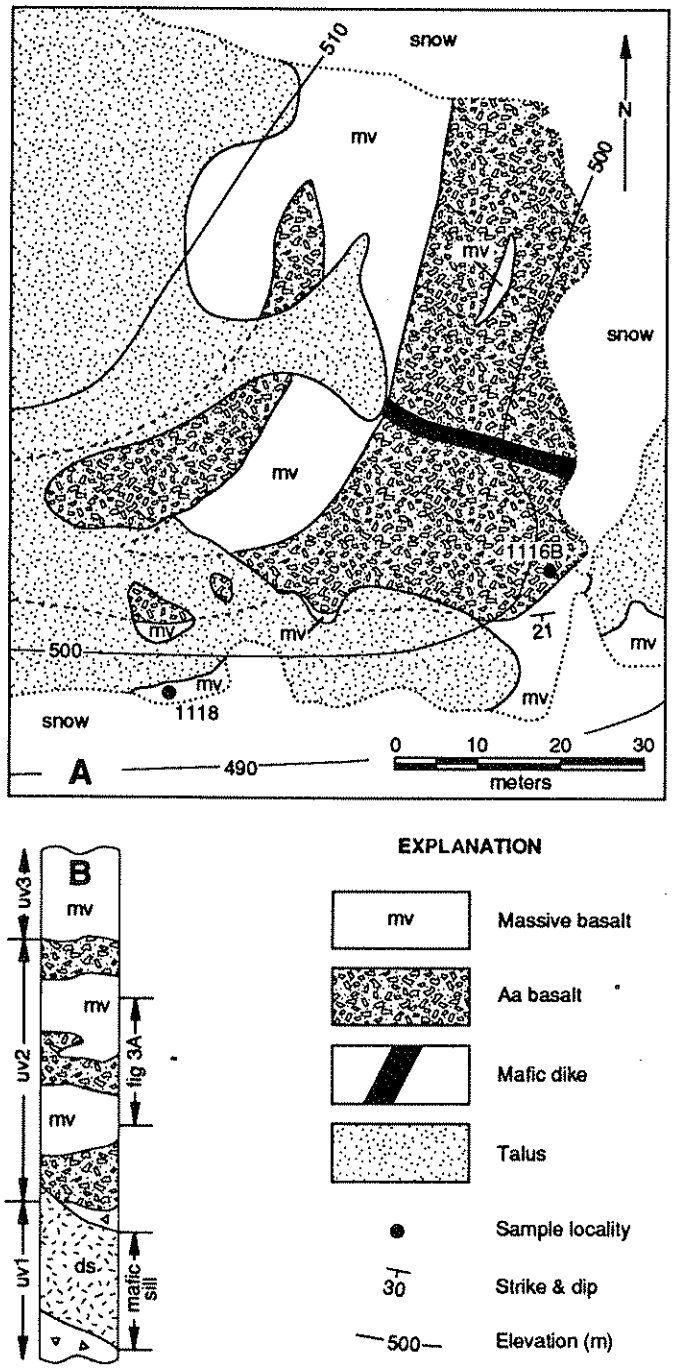

Figure 3. A: Geologic sketch map of aa unit uv2. See Figure 1 for location. Modal volumes and oxygen isotope ratios were determined for samples shown by filled circles. B: Schematic cross section showing the location of A relative to other map units (see Fig. 2). The cross section illustrates the irregular interbedding of massive and brecciated basalt within aa units.

Macroscopic primary porosities in massive units range from 0.6% to 10.5% and average 4%. Aa units have higher values of 1.8% to 22% and an average of 11%. The wider range in aa basalts reflects the heterogeneous primary porosity distribution caused by gradations from massive to brecciated zones. A sketch map of aa unit uv2 (Fig. 3) illustrates the alternating, irregular sequences of massive and brecciated basalt in this flow morphology. The massive portions of aa typically contain few vesicles. In contrast, massive flows (Fig. 2) display concentrations of vesicles at their bases and tops (Manning and Bird, 1991). The lithologies thus define a sequence of horizontal, bedding-controlled high- and low-porosity units. The two hydrostratigraphic units occupy approximately equal proportions of the aureole (Fig. 2).

METAMORPHISM

Methods of investigation

We investigated the influence of hydrologic properties on basalt metamorphism by comparing clasts from high-porosity aa units with low-porosity massive lavas. Samples of massive units were taken from the central portions of aa flows and from massive basalt flows. Samples of aa lavas were individual aa clasts extracted with a diamond saw. We obtained thin sections from a portion of each sample, and ran the remainder through a tungsten-carbide jaw crusher. Pieces containing macroscopic pores filled by secondary minerals were removed so that all analyses were of metabasalt matrices alone. The sorted pieces were powdered in a tungsten-carbide shatterbox and oxygen isotope ratios were obtained from splits of this material. Manning (1989) reported bulk densities, loss on ignition, and major and minor element geochemistry for these samples.

We determined mineral modes for representative samples (Table 1; see Figs. 2 and 3 for locations) by counting 2000 points on grids on three or four back-scattered electron photomicrographs. Magnifications were 72 to 300 times, depending on grain size. The locations of the photomicrographs were chosen randomly. When the textures or gray-scale intensities were ambiguous, we identified minerals by energy dispersive analysis.

Mineral compositions were determined by electron microprobe analysis. We used the following operating conditions: 15 kv accelerating potential, 15 na on faraday cup, ~1 μm beam size (10 μm for feldspars), and 30 s counting times.

TABLE 1. MODAL MINERALOGY AND $\delta^{18}O_{rock}$ OF REPRESENTATIVE SAMPLES*

Mineral zone	Actinolite + Chlorite			Pyroxene								Olivine	
Sample type	Aa	Massive		Aa					Massive			Aa	Mv
Sample number	1116B-1	1118	1133	1137A	1183	1321	1169-1	1339-4	1323	1173	1340	1185K	1185M
Distance	420	390	249	235	219	155	133	55	240	140	54	3	5
Magmatic phases													
Clinopyroxene	tr	2.7	13.9							tr		tr	tr
Plagioclase		39.7	47.6										
Titanomagnetite		tr	tr	0.2	0.7								
Metamorphic phases													
Actinolite	tr	46.0	28.6	*3.0*	*4.6*	*45.8*	*0.5*	*1.0*	*1.4*	*tr*	*0.1*		
Chlorite	37.0	1.0	tr	*28.5*	*28.0*	*0.2*	*1.4*	*0.8*	*9.5*	*tr0.4*			
Titanite	6.4	5.1	2.6	*3.6*	*9.0*	*1.8*	*tr*	*1.5*					
Epidote	0.5			*tr*									
Quartz	26.3	tr	tr	*trtr*	*tr2.1*		*2.5*						
Calcite	9.9			*2.8*									
Na plagioclase	17.8	tr	tr	*47.4*	*trtr*			*1.1*					
K feldspar		tr		*5.6*	*3.2*			*0.2*		*tr*			
Labradorite					44.5	43.9	50.6	50.5	43.9	47.7	47.6	55.9	56.3
Clinopyroxene				8.6	9.8	2.4	37.5	32.2	37.1	30.7	34.1	21.2	31.4
Orthopyroxene							0.7	9.0		15.8	15.9	15.9	1.9
Biotite							tr	2.7		tr	0.8		
Olivine												tr	7.6
Magnetite		5.3	4.5										*tr*
Ilmenite			2.7			5.8	7.1	3.5	2.9	5.7	5.2	5.1	2.4
Other	1.9											*1.6*	*0.3*
$\delta^{18}O_{rock}$ (‰)	2.6	2.4	3.5	1.8	1.7	2.0	2.4	1.9	1.9	2.5	2.6	3.0	2.0

*Modal volumes (%). Retrograde phases are italicized. Distances are from contact in meters. Abbreviations: Mv = massive; tr = trace (<0.1%). Other phases: trace zircon in all samples; trace Cu-Fe sulfide in 1116B-1 and 1340, and 1.9% rutile in 1116B, 0.3% talc in 1185M, and 1.6% cummingtonite in 1185K.

Well-characterized silicates and oxides were employed as standards, and oxide sums were calculated using a Bence-Albee (1968) matrix-correction algorithm (Chambers, 1985).

Oxygen isotope ratios are reported relative to standard mean ocean water and have precisions of ±0.1‰ based on replicate analyses of silicate standards.

Mineral zones

Metamorphic grade increases toward the Skaergaard intrusion, although local contact metamorphism also occurs in coastal areas where dike densities are high (Bird et al., unpublished data). Coexisting pore-filling index minerals and characteristic textures define five mineral zones: the prehnite + calcite zone, the prehnite + epidote zone, the actinolite + chlorite zone, the pyroxene zone, and the olivine zone (Bird et al., 1988; Manning, 1989; Manning and Bird, 1991). The prehnite + calcite and prehnite + epidote zones do not occur in the area investigated in this study (Fig. 1). The prehnite + calcite zone occurs beyond ~14 km from the contact, where secondary minerals filling pores and partially replacing magmatic clinopyroxene, plagioclase, and Fe-Ti oxides include prehnite, calcite, chlorite, quartz, K-feldspar, albite, zeolites, and titanite. This zone continues northward and upsection into basalts characterized by zeolite zones similar to those described by Walker (1960) in Iceland (Larsen et al., 1989). Between about 2 and 14 km from the intrusion the same mineral assemblage is found, except that epidote occurs instead of zeolites, defining the prehnite + epidote zone (Fig. 1). This zone corresponds to the prehnite-actinolite facies of Liou et al. (1985), although coexisting prehnite and actinolite are rare in vugs and vesicles.

Actinolite + chlorite zone. Between 0.25 and ~2 km from the contact, the magmatic mineral assemblage is partially replaced by actinolite, chlorite, quartz, sodic plagioclase, and titanite (Table 1). The secondary mineral assemblage also includes sporadic K-feldspar, rutile, zircon, and calcite. Primary pores such as vesicles and breccia interspace are filled by combinations of most of these minerals, as well as grandite garnet, Cu-Fe sulfides, and rare clinopyroxene. Both the matrix and pore-filling mineral assemblages in the actinolite + chlorite zone are consistent with those of the greenschist facies of Liou et al. (1985). On the basis of metamorphic mineral compositions (see below), the actinolite + chlorite zone near its boundary with the pyroxene zone records the uppermost greenschist facies where it is transitional to the amphibolite facies (e.g., Maruyama et al., 1983). Manning et al. (1993) suggested that the minerals of the actinolite + chlorite zone formed between 300 and 550 °C.

The textures of massive units and aa clasts differ in this zone (Figs. 4A and 5A). In the massive units, lath-shaped plagioclase, variably pseudomorphed intergranular clinopyroxene, and equant titanomagnetite define a relict magmatic texture (Fig. 4A). Although all samples are at least partly altered, the intergranular textures of massive basalts suggest that their protoliths were holocrystalline. Massive units have small modal volumes of magmatic clinopyroxene and large modal volumes of actinolite (Table 1). Magmatic plagioclase is common, but small amounts are altered to sodic plagioclase at grain margins in all samples studied. In addition, modal volumes of chlorite are low, and magnetite and/or ilmenite occur with titanite as alteration of magmatic titanomagnetite.

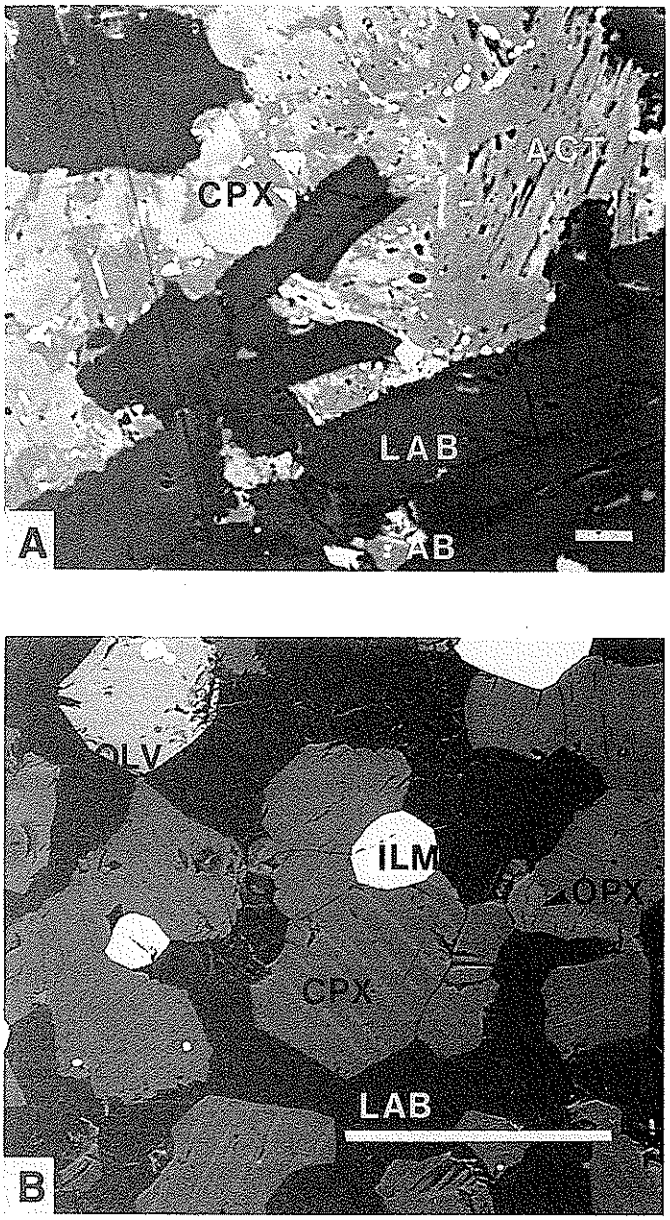

Figure 4. Back-scattered electron photomicrographs showing textures of massive samples. A: Sample 1133 from the actinolite + chlorite zone; B: sample 1185M from the olivine zone. See Figure 2 for sample locations. Scale bars are 10 μm in A and 100 μm in B. Mineral abbreviations: CPX, clinopyroxene; ACT, actinolite; LAB, labradorite; AB, albite/oligoclase; OLV, olivine; OPX, orthopyroxene; ILM, ilmenite.

In contrast to the massive lithologies, aa clasts only rarely display igneous textures (Fig. 5A) and chlorite is more abundant than actinolite (Table 1). Figure 5B shows an aa clast from the prehnite + calcite zone ~20 km east of the contact that is less altered than samples from the study area. Chlorite surrounds equant, locally subhedral, fine-grained augite and lath-shaped plagioclase, suggesting the presence of basaltic glass in clast protoliths. In the study area, the ratio of chlorite to actinolite is higher in aa clasts than in massive samples, probably because of alteration of this glass to chlorite. In addition, the low modal volumes of magmatic phases relative to the massive lavas (Table 1) suggest that mineralogic alteration of aa clasts was more extensive than massive samples. Unlike in massive lithologies, calcite and rutile occur sporadically in aa clasts and magnetite and ilmenite are absent (Table 1).

Pyroxene zone. Within 250 m from the contact both aa clasts and massive units have granoblastic-polygonal textures, with predominantly lath-shaped plagioclase and equant pyroxene and Fe-Ti oxide grains (Fig. 5C). Minerals diagnostic of the pyroxene zone are clinopyroxene, labradorite, and ilmenite (Table 1). Biotite and orthopyroxene are ubiquitous minor phases within ~150 m from the contact but are rare or absent beyond this distance. The only parts of pyroxene zone rocks that were not recrystallized are rare phenocrysts of plagioclase and clinopyroxene. As noted by Manning and Bird (1991), primary pore space in the pyroxene zone is filled by the same mineral assemblage found in metabasalt matrices. Minimum temperatures of metamorphism derived from pyroxene equilibria (Anderson et al., 1993) decrease from 900 ± 50 °C at 10 m to 750 ± 50°C at 250 m from the contact (Manning et al., 1993). In contrast to the actinolite + chlorite zone, mineral identities and abundances in the pyroxene zone are similar in aa and massive samples.

The mineral assemblage that defines the actinolite + chlorite zone overgrows and thus postdates the high-temperature assemblage throughout the pyroxene zone. For example, Figure 5D shows granoblastic-polygonal metamorphic clinopyroxene that was replaced by actinolite, chlorite, and minor cummingtonite. Metamorphic labradorite is also partially altered to sodic plagioclase at grain margins. Between 200 and 250 m from the contact, this retrograde alteration may be so extensive (up to ~90%; Table 1) that it obscures the boundary between the actinolite + chlorite and pyroxene zones, making it impossible to discern in the field or in thin section whether the protolith was fresh basalt or pyroxene zone hornfels. However, as discussed below, igneous clinopyroxenes are distinctly less calcic than metamorphic clinopyroxenes in the study area, and electron microprobe analyses show that clinopyroxenes between 200 and 250 m from the contact are metamorphic. This differs from our earlier assessment of the

boundary between the actinolite + chlorite and pyroxene zones at 210 m from the contact (Manning and Bird, 1991), which was based solely on textural criteria and thus overlooked the outermost 40 m of the pyroxene zone.

Olivine zone. Metamorphic olivine occurs with pyroxene zone mineral assemblages within 10 m of the contact (Table 1; Fig. 4B). Rocks from this zone are coarse-grained hornfelses with common porphyroblasts of clinopyroxene and biotite. On the basis of major and minor element geochemistry and metamorphic temperatures, Manning (1989) concluded that olivine zone metabasalts partially melted at peak metamorphic conditions.

Mineral compositions

Representative mineral compositions are given in Tables 2 through 5 and discussed below. Except for chlorite, compositions of minerals in massive samples do not differ from those in aa samples.

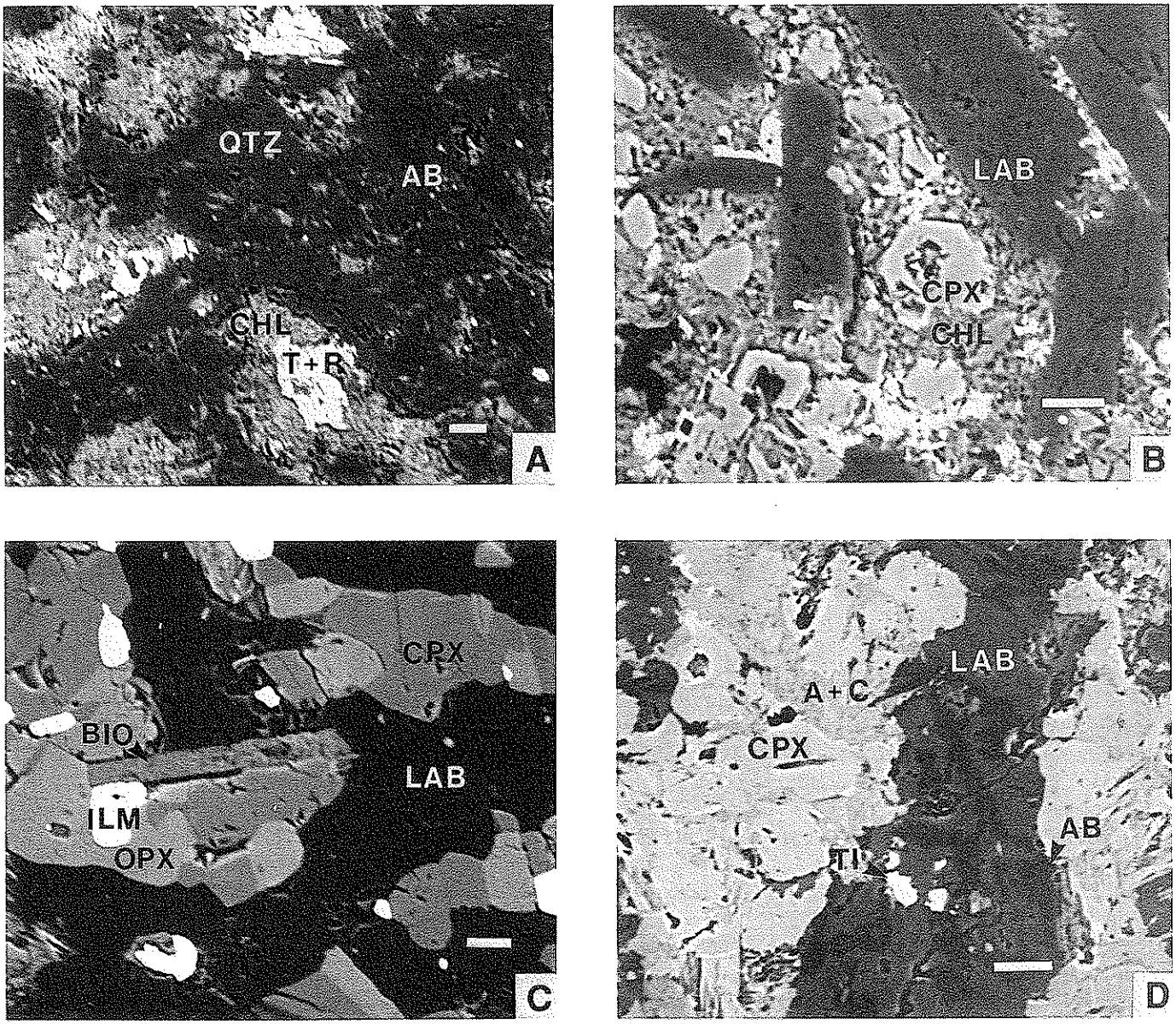

Figure 5. Back-scattered electron photomicrographs showing textures of aa clast samples. A: Sample 1116B-1 from the actinolite + chlorite zone; B: aa clast from the prehnite + calcite zone ~20 km east of the contact; C: sample 1339-4 from the pyroxene zone; D: sample 1321 showing retrograde alteration of the pyroxene zone mineral assemblage to those of the actinolite + chlorite zone. See Figures 2 and 3 for sample localities. All scale bars are 10 μm. Mineral abbreviations: T + R, titanite + rutile; TI, titanite; CHL, chlorite; QTZ, quartz; AB, albite/oligoclase; A + C, actinolite + chlorite; CPX, clinopyroxene; LAB, labradorite; BIO, biotite; OPX, orthopyroxene; ILM, ilmenite.

TABLE 2. REPRESENTATIVE FELDSPAR COMPOSITIONS*

	Actinolite + Chlorite			Pyroxene						Olivine
Sample	1118	1118	1118	1323	1323	1321	1321	1169-1	1340	1185K
Distance	390	390	390	240	240	155	155	133	54	3
Analysis	7(m)	10	8	13	15(r)	11	12(r)	4	1	1
SiO_2	52.7	64.2	64.1	53.6 (2)	62.3	53.5	65.8	52.5	52.7	52.4
TiO_2	0.15	0.05	0.04	0.16(2)	0.09	0.06	0.11	0.15	b.d.	0.11
Al_2O_3	28.7	21.5	18.2	28.6 (1)	21.3	29.2	21.6	29.6	29.4	29.7
Fe_2O_3	1.31	0.36	0.41	0.66(3)	1.49	0.46	0.34	0.48	0.44	0.31
MgO	0.18	0.05	0.09	0.26(1)	0.67	0.01	0.01	0.09	0.01	0.02
CaO	12.4	2.83	0.60	11.6 (1)	2.77	11.6	2.77	12.3	12.1	12.8
Na_2O	4.34	10.3	0.51	4.69(7)	9.6	4.73	10.4	4.16	4.52	4.22
K_2O	0.14	0.15	15.4	0.21(2)	0.10	0.27	0.11	0.31	0.18	0.17
Total	99.9	99.4	99.4	99.8	98.3	99.8	101.1	99.6	99.4	99.7
Si	2.40	2.85	2.98	2.43	2.81	2.43	2.87	2.39	2.40	2.39
Ti	0.01	0.00	0.00	0.01	0.00	0.00	0.00	0.01	0.00	0.00
Al	1.54	1.13	1.00	1.53	1.13	1.56	1.11	1.59	1.58	1.59
Fe^{3+}	0.04	0.01	0.01	0.02	0.05	0.02	0.01	0.02	0.02	0.01
Mg	0.01	0.00	0.01	0.02	0.04	0.00	0.00	0.01	0.00	0.00
Ca	0.61	0.13	0.03	0.56	0.13	0.56	0.13	0.60	0.59	0.63
Na	0.38	0.89	0.05	0.41	0.84	0.42	0.88	0.37	0.40	0.37
K	0.00	0.01	0.91	0.01	0.01	0.02	0.01	0.02	0.01	0.01
Total	4.99	5.02	4.99	4.99	5.01	5.01	5.01	5.01	5.00	5.00

*Analyses represent prograde metamorphic feldspars unless designated magmatic (m) or retrograde (r). Distances are from the contact in meters. Oxides in weight percent; formulae based on eight oxygens. Numbers in parentheses are representative uncertainties in last digit based on 1σ counting errors. Abbreviation: b.d. = below detection.

Feldspar. Magmatic plagioclase in the actinolite + chlorite zone is labradorite in composition (X_{An} = 0.51 to 0.66, where $X_{An} = n_{Ca}/[n_{Ca} + n_{Na} + n_K]$ and n is atoms per eight oxygens; Fig. 6A, Table 2). Metamorphic plagioclase in the pyroxene zone has a similar spread in anorthite content (X_{An} = 0.50 to 0.65; Table 2). Analyses from a single sample suggest that metamorphic plagioclase in the actinolite + chlorite zone mineral assemblages is oligoclase (X_{An} = 0.13 to 0.19). Retrograde plagioclase replacing metamorphic labradorite in the pyroxene zone ranges to somewhat lower X_{An} (0.07 to 0.19). Figure 6A shows that there is no difference in X_{An} between plagioclase from aa and massive units throughout the aureole. Potassium feldspars occur only in the actinolite + chlorite zone and are nearly stoichiometric.

Pyroxene and olivine. Clinopyroxene compositions are important in differentiating between the pyroxene and actinolite + chlorite zones (Fig. 6B). Only relict igneous clinopyroxenes occur in the actinolite + chlorite zone. They can be distinguished by their high minor element contents and low X_{Ca} of 0.37 to 0.40, where $X_{Ca} = n_{Ca}/[n_{Ca} + n_{Fe2+} + n_{Mg}]$ and n is atoms per six oxygens (Table 3). Metamorphic clinopyroxenes in the pyroxene zone have higher X_{Ca} (Fig. 6B) and lower minor element contents. Similar characteristics differentiate magmatic and secondary clinopyroxenes at the margins of hydrothermal veins within the Skaergaard intrusion (Manning and Bird, 1986). In the pyroxene zone, X_{Mg} ($X_{Mg} = n_{Mg}/[n_{Mg} + n_{Fe2+}]$) ranges from 0.65 to 0.75. Although complicated by exsolution near the contact, X_{Ca} in metamorphic clinopyroxene within the pyroxene zone decreases with decreasing distance from the contact (Fig. 6B), consistent with increasing peak metamorphic temperatures as the contact is approached (Manning et al., 1993). Between 225 and 250 m from the contact, both metamorphic and magmatic clinopyroxenes may display a somewhat wider range in X_{Ca}. We interpret this feature of the outermost pyroxene zone to reflect partially exchanged, disequilibrium clinopyroxene compositions.

Measured values of X_{Ca} in orthopyroxenes increase from ~0.02 in the pyroxene zone to a maximum of 0.09 in the olivine zone (Table 3). Values of X_{Mg} exhibit a similar trend, increasing from ~0.55 in the pyroxene zone to 0.61 in the olivine zone. Many orthopyroxenes in the olivine zone contain blebby exsolution lamellae of clinopyroxene and have compositions that reflect reequilibration at lower temperatures. Values of X_{Mg} in olivines from the olivine zone are 0.55 to 0.48.

Comparison of clinopyroxene (Fig. 6B), orthopyroxene, and olivine compositions from the two basalt morphologies reveals no systematic differences.

Biotite. Assuming the total analyzed iron is ferrous, the

TABLE 3. REPRESENTATIVE PYROXENE AND OLIVINE COMPOSITIONS*

	Clinopyroxene						Orthopyroxene				Olivine	
Mineral zone	Act+Chl	Pyroxene				Olivine	Pyroxene		Olivine		Olivine	
Sample	1118	1323	1321	1169-1	1340	1185K	1165	1340	1185K	644E	644E	644C
Distance	390	240	155	133	54	3	131	54	2	0.15	0.15	2
Analysis	19(m)	10	6	1	6	9	a16	8	6	a12	a27	a17
SiO_2	51.7	53.0 (2)	53.9	52.7	52.7	52.1	53.7 (2)	51.6	53.2	53.8	35.6 (2)	35.6
Al_2O_3	2.48	0.33 (2)	0.56	0.74	0.67	1.54	0.42 (2)	0.40	0.50	0.67	0.02 (1)	b.d.
FeO	9.3	11.6 (1)	8.9	12.0	11.9	11.8	25.5 (3)	27.7	23.7	23.2	39.3 (2)	41.8
MgO	17.1	13.2 (1)	14.3	12.9	13.4	14.5	19.5 (2)	18.3	21.6	21.2	26.7 (2)	22.4
CaO	18.1	20.7 (1)	22.2	21.1	21.2	19.2	1.20 (4)	1.24	0.95	1.89	0.03 (2)	0.08
Na_2O	0.19	0.17 (2)	0.19	0.20	0.24	0.11	b.d.	b.d.	b.d.	b.d.	b.d.	b.d.
TiO_2	0.97	0.06 (4)	0.27	0.22	0.25	0.54	0.11 (3)	0.26	0.30	0.51	0.03 (2)	0.08
MnO	0.17	0.21 (3)	0.17	0.43	0.19	0.20	0.42 (3)	0.41	0.32	0.28	0.35 (3)	0.50
Total	100.0	99.3	100.5	100.3	100.6	100.0	100.9	99.9	101.6	100.6	102.0	100.5
Si	1.91	2.00	1.99	1.98	1.97	1.95	2.01	1.98	1.98	1.98	0.99	1.02
Al	0.11	0.02	0.02	0.03	0.03	0.07	0.02	0.02	0.02	0.03	0.00	0.00
Fe^{3+}	0.04	0.00	0.00	0.01	0.03	0.01	0.00	0.00	0.00	0.00		
Fe^{2+}	0.24	0.37	0.28	0.37	0.34	0.36	0.80	0.89	0.74	0.71	0.91	1.00
Mg	0.94	0.75	0.79	0.72	0.75	0.81	1.09	1.04	1.20	1.16	1.10	0.95
Ca	0.72	0.84	0.88	0.85	0.85	0.77	0.05	0.05	0.04	0.07	0.00	0.00
Na	0.01	0.01	0.01	0.01	0.02	0.01						
Ti	0.03	0.00	0.01	0.01	0.01	0.02	0.00	0.01	0.01	0.01	0.00	0.00
Mn	0.01	0.01	0.01	0.01	0.01	0.01	0.01	0.01	0.01	0.01	0.01	0.01
Total	4.01	4.00	3.99	3.99	4.01	4.01	3.98	4.00	4.00	3.97	3.01	2.98

*Analyses represent prograde metamorphic minerals unless designated magmatic (m). Distances are from the contact in meters. Oxides in weight percent; formulae based on six, three, and four oxygens for clinopyroxenes, orthopyroxenes, and olivines, respectively. Fe^{3+} in pyroxenes calculated by charge balance. Numbers in parentheses are representative uncertainties in last digit based on 1σ counting errors. Abbreviations: Act + Chl = actinolite + chlorite zone; b.d. = below detection; n.a. = not analyzed.

maximum observed octahedral Al content is 0.09 atoms per 11 anhydrous oxygens in metamorphic biotites. Values of X_{Mg} increase toward the contact from 0.38 at 190 m to 0.63 at the contact (Table 4). Titanium contents are high and also increase toward the contact. High Ti concentrations are consistent with the presence of ilmenite in the assemblage (e.g., Guidotti, 1984).

Amphibole. Figure 7A shows that calcic amphiboles in the actinolite + chlorite zone have X_{Mg} = 0.71 to 0.79 and tetrahedral aluminum (^{IV}Al) contents of 0.21 to 0.44 atoms per 23 anhydrous oxygens. Where they form as retrograde alteration of pyroxene zone mineral assemblages, calcic amphiboles have a much wider range in composition (Fig. 7A). Compositions are predominantly actinolites in the nomenclature of Leake (1978), but compositions include ferro-actinolite and actinolitic hornblende. Retrograde calcic amphiboles in the pyroxene and olivine zones may coexist with cummingtonite (X_{Mg} = 0.45), which forms as a local alteration product of olivine and orthopyroxene. Figure 7A shows that there is no difference between retrograde calcic amphiboles from aa and massive units. Representative compositions are given in Table 4.

No amphibole compositions more aluminous than ^{IV}Al = 0.75 were found in the study area. The metabasalts that host the Cuillen gabbros of Skye, Scotland (Ferry et al., 1987), contain only uncommon edenitic hornblendes. The absence or low abundance of hornblende at these localities probably resulted from the fresh basalt protoliths and low rates of hornblende nucleation (Manning et al., 1993).

Chlorite. Chlorites in the actinolite + chlorite zone have X_{Fe} of 0.30 to 0.64, where $X_{Fe} = n_{Fe}/(n_{Fe} + n_{Mg})$ and n is atoms per 14 anhydrous oxygens. Values of n_{Si} are 2.79 to 3.10 (Fig. 7B). Chlorites are thus Fe clinochlores and Mg chamosites in the nomenclature of Bayliss (1975). Figure 7B suggests that Fe and Al covary in prograde chlorites. Retrograde chlorite compositions in the pyroxene zone have a narrower range in X_{Fe} and a much wider range in Si content, and Fe and Al do not correlate in late chlorites. The limited data presented in Figure 7B suggest that, in the actinolite + chlorite zone, chlorites from massive units are more Fe and Al rich than their counterparts from aa units; however, the significance of this is unclear. Representative compositions are given in Table 4.

Fe-Ti oxide. Table 5 shows that, in the actinolite + chlorite zone, magmatic titanomagnetites are ulvöspinel-rich solid solutions (72.0% Fe_2TiO_4; analysis 1118-25). Secondary Fe-Ti oxides in this zone are magnetite rich (97.6% Fe_3O_4; analysis

TABLE 4. REPRESENTATIVE AMPHIBOLE, CHLORITE, AND BIOTITE COMPOSITIONS*

	Amphibole				Chlorite				Biotite				
Mineral zone	Act+Chl		Pyroxene		Act+Chl		Pyroxene		Pyroxene				Olivine
Sample	1118	1133	1321	1176	1116B-1	1118	1323	1321	1176	1174	1165	1340	644E
Distance	390	249	155	188	420	390	240	155	188	163	131	54	0.15
Analysis	3	26	7(r)	d3(r)	2	16	1(r)	14(r)	d1	a18	a9	3	a21
SiO_2	54.2 (2)	53.4	52.3	52.6	28.4 (1)	26.1	28.2	28.2	36.4 (1)	36.1	37.4	36.9	37.9
TiO_2	0.33 (5)	0.42	0.16	0.25	b.d.	b.d.	0.10	b.d.	5.4 (2)	5.1	5.0	6.1	7.0
Al_2O_3	2.86 (3)	2.98	4.50	2.03	18.7 (1)	19.1	15.7	18.2	14.1 (1)	13.5	13.8	13.7	13.8
FeO	12.0 (2)	10.1	12.2	21.4	23.0 (2)	32.2	26.3	21.6	22.9 (2)	24.2	18.8	17.6	14.1
MgO	17.0 (1)	17.1	15.4	10.8	19.6 (2)	11.2	16.3	19.9	8.7 (1)	8.5	11.4	12.3	13.5
MnO	0.33 (3)	0.20	0.27	0.34	0.11 (2)	0.28	0.13	0.16	0.07 (2)	0.07	0.06	0.03	0.06
CaO	10.47 (8)	12.23	11.89	10.00	0.05 (1)	0.21	0.20	0.12	0.09 (1)	0.01	0.17	0.03	0.08
Na_2O	0.18 (3)	0.36	0.68	0.34	b.d	b.d.	b.d.	b.d.	0.36 (3)	0.22	0.44	0.31	0.23
K_2O	0.01 (1)	0.14	b.d	0.02	b.d.	b.d.	n.a.	n.d.	9.3 (1)	9.2	9.0	9.0	9.4
Total	97.4	97.0	97.3	97.8	89.9	89.1	86.9	88.2	97.3	96.9	96.1	96.0	96.1
Si	7.74	7.63	7.50	7.83	2.87	2.81	3.00	2.89	2.78	2.78	2.82	2.78	2.78
Ti	0.04	0.05	0.03	0.03	0.00	0.00	0.01	0.00	0.31	0.29	0.29	0.34	0.39
Al	0.48	0.50	0.76	0.36	2.24	2.42	1.97	2.20	1.27	1.22	1.22	1.21	1.20
Fe^{3+}	0.01	0.12	0.22	0.01									
Fe^{2+}	1.43	1.09	1.24	2.65	1.95	2.90	2.34	1.85	1.46	1.56	1.18	1.11	0.87
Mg	3.61	3.64	3.28	2.39	2.95	1.79	2.65	3.04	0.99	0.90	1.28	1.38	1.49
Mn	0.04	0.02	0.03	0.04	0.01	0.03	0.01	0.01	0.01	0.01	0.00	0.00	0.00
Ca	1.60	1.87	1.83	1.59	0.01	0.02	0.02	0.01	0.01	0.01	0.01	0.00	0.01
Na	0.04	0.10	0.19	0.10	0.00	0.00	0.00	0.00	0.05	0.03	0.06	0.04	0.03
K	0.00	0.03	0.00	0.00	0.00	0.00	0.00	0.00	0.90	0.91	0.87	0.86	0.88
Total	14.99	15.05	15.08	15.00	10.03	9.97	10.01	10.00	7.78	7.71	7.73	7.72	7.65

*Analyses represent prograde metamorphic minerals unless designated retrograde (r). Distances are from the contact in meters. Oxides in weight percent; formulae based on 23, 14, or 11 anhydrous oxygens for amphiboles, chlorites, and biotites, respectively. All Fe assumed to be Fe^{2+} except in amphiboles, for which Fe^{3+} was calculated by charge balance. Numbers in parentheses are representative uncertainties in last digit based on 1σ counting errors. Abbreviations as in Table 3.

1118-24). Iron-titanium oxide compositions in the pyroxene and olivine zones are nearly pure ilmenite (96.9%–97.9% $FeTiO_3$).

Other phases. Energy dispersive X-ray spectra showed titanite, zircon, calcite, rutile, and quartz to be stoichiometric.

Extent of metamorphism

The samples shown in Figures 2 and 3 were studied to identify possible correlations between extent of metamorphism and macroscopic primary porosity. Where bulk compositions and mineral assemblages are well constrained, specific mineral-fluid reactions allow quantitative determination of reaction progress (e.g., Ferry, 1986); however, complex solid solutions of variable composition and uncertain starting mineral abundances in the basalts preclude such a treatment in this study. Instead, we used two alteration indices (AI) to characterize the extent of metamorphism.

In the pyroxene and olivine zones, retrograde alteration between 200 and 250 m from the contact complicates the determination of extent of metamorphism. Where retrograde alteration is pervasive, magmatic textures cannot be discerned from metamorphic textures. However, X_{Ca} of magmatic and metamorphic clinopyroxenes are distinct. Except for those within several meters of the contact, all metamorphic clinopyroxenes have $X_{Ca} > 0.40$, whereas clinopyroxenes in samples with unambiguous magmatic textures have $X_{Ca} < 0.40$ (Fig. 6B). This difference is independent of the amount of retrograde alteration, so we can exploit clinopyroxene compositions to evaluate the extents of metamorphic reactions that produced olivine and pyroxene zone mineral assemblages. Using 10 to 20 analyzed mineral grains, we defined AI_{pyx} for each sample as the number of clinopyroxene grains with $X_{Ca} > 0.40$ divided by the total number of clinopyroxene grains analyzed.

Values of AI_{pyx} are 1.0 in both lithologies in the pyroxene and olivine zones (Fig. 8A). There is therefore no difference in the extent of prograde mineralogic reactions between aa and massive lithologies, and prograde reactions proceeded to completion within 240 m. However, between 240 and 250 m, clinopyroxene analyses interpreted as both magmatic and metamorphic occur in two samples (Fig. 6B), suggesting that in the outermost 10 m of the pyroxene zone, reactions producing metamorphic clinopyroxenes were incomplete.

TABLE 5. REPRESENTATIVE Fe-Ti OXIDE COMPOSITIONS*

Mineral zone	Act + Chl		Pyroxene				Olivine
Sample	1118	1118	1323	1321	1165	1340	1185K
Distance	390	390	240	155	131	54	3
Analysis	24	25(m)	16	15	14	10	11
SiO_2	0.18	0.24 (2)	0.08	0.08	0.05	0.07	0.03
TiO_2	0.82	24.9 (2)	49.9	51.1	50.0	50.0	50.3
Al_2O_3	0.01	0.03 (1)	b.d.	0.06	b.d.	0.04	0.03
Cr_2O_3	0.05	0.04 (1)	0.30	0.12	0.06	0.13	0.35
Fe_2O_3	66.3	18.3 (1)	2.0	2.2	3.1	2.1	3.1
FeO	31.8	51.4 (3)	42.4	43.0	44.0	44.3	44.3
MgO	b.d.	b.d.	0.07	0.04	0.05	0.09	0.08
MnO	b.d.	2.14 (5)	2.35	2.92	1.66	0.90	0.87
CaO	b.d.	b.d.	b.d.	b.d.	0.26	b.d.	b.d.
Total	99.2	97.1	97.1	99.5	99.2	97.6	99.1
Si	0.01	0.01	0.00	0.00	0.00	0.00	0.00
Ti	0.02	0.72	0.97	0.98	0.97	0.98	0.97
Al	0.00	0.00	0.00	0.00	0.00	0.00	0.00
Cr	0.00	0.00	0.01	0.00	0.00	0.00	0.00
Fe^{3+}	1.94	0.53	0.04	0.04	0.06	0.04	0.06
Fe^{2+}	1.03	1.66	0.92	0.91	0.92	0.95	0.94
Mg	0.00	0.00	0.00	0.00	0.00	0.00	0.00
Mn	0.00	0.07	0.05	0.06	0.04	0.02	0.02
Ca	0.00	0.00	0.00	0.00	0.01	0.00	0.00
Total	3.00	2.99	1.99	1.99	2.00	1.99	1.99

*Analyses represent progade metamorphic minerals unless designated magmatic (m). Distances are from the contact in meters. Oxides in weight percent; formulae based on four or three oxygens for magnetites and ilmenites, respectively. Fe^{3+} calculated by charge balance. Numbers in parentheses are representative uncertainties in last digit based on 1σ counting errors. Abbreviations as in Table 3.

Minerals of the actinolite + chlorite zone were the only secondary phases to form beyond 250 m. They also formed during retrograde alteration of the pyroxene and olivine zones within 250 m of the contact. To evaluate the extent of these reactions we defined AI_{acz} as the sum of the modal volumes of actinolite + chlorite zone minerals (actinolite, chlorite, titanite, epidote, quartz, calcite, albite, and K-feldspar) divided by the modal volume of all minerals other than Fe-Ti oxides. Fe-Ti oxides were excluded because magnetite and ilmenite may have formed during both prograde and retrograde metamorphism (Table 1). Ferry (1985) used a similar measure in his study of gabbro alteration. Values of AI_{acz} are plotted in Figure 8B as a function of distance from the contact. Although we have few data from the actinolite + chlorite zone, the figure suggests that AI_{acz} in the aa sample is much higher than AI_{acz} in the massive samples. Figure 8B also shows that the extent of retrograde reactions that formed actinolite + chlorite zone minerals in the pyroxene and olivine zones decreases as the contact is approached, and is higher in aa than in massive samples at any given distance. The magnitude of the difference, however, decreases as the contact is approached.

Oxygen isotope geochemistry

Taylor and Forester (1979) used deuterium/hydrogen (D/H) and $^{18}O/^{16}O$ to infer that the circulating water in the magma-hydrothermal system was meteoric in origin. As part of their study, they obtained whole-rock $\delta^{18}O$ values of 1.3‰ to 2.5‰ (mean 1.9‰) for six basalts <1 km from the eastern contact. Table 1 and Figure 9 give our analyses of $\delta^{18}O_{rock}$ for representative massive and aa clast samples. Samples of the olivine zone are excluded because of the unknown extent of partial melting there (Manning, 1989). Our analyses range more widely (1.7‰ to 3.5‰) and have a higher mean (2.3‰) than Taylor and Forester's (1979). This could be because most of their samples were from the volcaniclastic breccia (uv1, Fig. 2), which we did not analyze, or because low $\delta^{18}O$ pore-filling minerals may have been present in their samples, or both.

The maximum $\delta^{18}O_{rock}$ in the prehnite + epidote and zones (Fig. 1) is ~4.5‰ (Taylor and Forester, 1979; Bird et al., unpublished data). The basalts were probably mineralogically unaltered prior to gabbro emplacement (Manning et al., 1993), and although the original magmatic $\delta^{18}O_{rock}$ compositions are

not known, there is no evidence to suggest that they were lower than the 5.7‰ value typical for fresh basalts (e.g., Taylor and Sheppard, 1986). Figure 9 therefore implies that $^{18}O/^{16}O$ in all basaltic lithologies decreased by ~2‰ to 4‰ through reaction with the meteoric water during metamorphism. Figure 9 also suggests that the data from each mineral zone define distinct groups. Analyses from the outermost pyroxene zone cluster at ~2.0‰. As the contact is approached, $\delta^{18}O_{rock}$ for massive samples increases slightly to 2.6‰ at 50 m. Values of $\delta^{18}O_{rock}$ are more scattered for aa samples, but at any given point in the pyroxene zone, they are similar to or lower than those of massive samples. Three analyses suggest that in the actinolite + chlorite zone there is a somewhat higher mean $\delta^{18}O_{rock}$ value, that $\delta^{18}O_{rock}$ increases as the contact is approached over the narrow interval of 250 m to 450 m, and that there is an abrupt change in $\delta^{18}O_{rock}$ at the mineral zone boundary. However, more analyses are required to confirm these observations.

The whole-rock isotopic data must be interpreted in light of the contrasting metamorphic histories in the two mineral zones. The pyroxene zone is characterized by complete prograde mineralogic reactions and textural equilibrium. Metamorphic temperatures exceeded ~700 °C (Manning et al., 1993). These observations suggest equilibrium $\delta^{18}O_{rock}$ compositions. However, the relict igneous minerals in the actino-

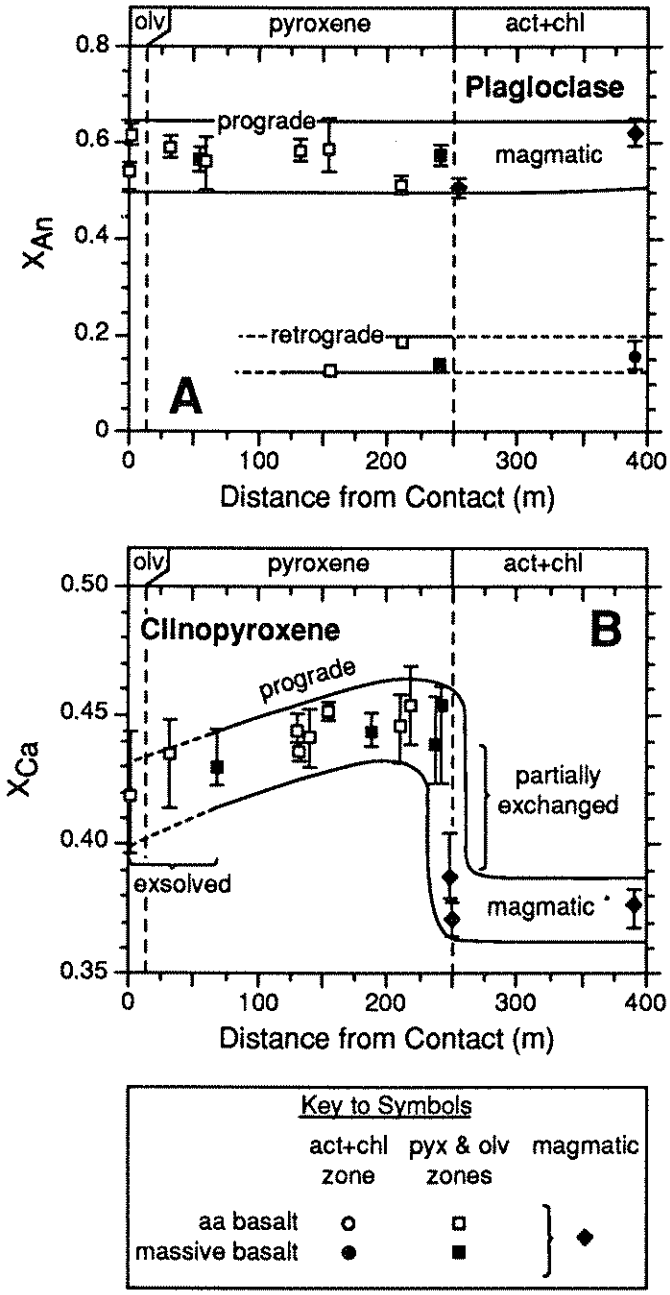

Figure 6. Variations in X_{An} in plagioclase (A) and X_{Ca} in clinopyroxene (B) with distance from the contact with the Skaergaard intrusion. Shown at the top of each plot are the mineral zones discussed in the text (olv, olivine zone; act + chl, actinolite + chlorite zone). Symbols are averages of all analyses for the sample and bars show the range in observed compositions.

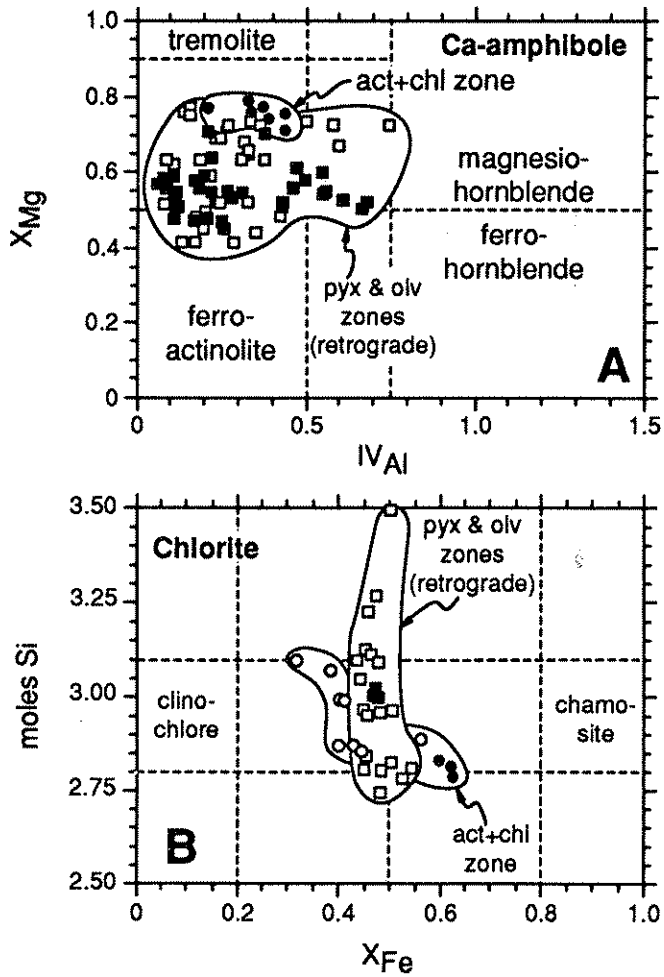

Figure 7. A: X_{Mg} vs. tetrahedral Al in calcic amphiboles. B: Moles of Si (per 14 anhydrous oxygens) vs. X_{Fe} in chlorites. Symbols are explained in Figure 6, except for pyx, pyroxene. Dashed lines are the compositional limits for the names of Leake (1978) and Bayliss (1975). Selected names of these phases are shown for reference.

lite + chlorite zone point to textural disequilibrium and incomplete metamorphic reactions at the 300–550 °C temperatures recorded by the mineral assemblage beyond 250 m. Manning et al. (1993) noted that temperatures in the portion of the actinolite + chlorite zone shown in Figure 9 probably exceeded 550 °C in the first ~30,000 yr of the system's history, but no mineralogic reaction occurred during this time. The mineralogic disequilibrium implied both by large temperature oversteps and by the preservation of relict igneous minerals suggests that whole-rock $^{18}O/^{16}O$ values in the actinolite + chlorite zone are not equilibrium values.

Isotopic disequilibrium is a common feature of hydrothermal alteration and metamorphism associated with the epizonal mafic systems of the North Atlantic Tertiary province and oceanic spreading centers (e.g., Forester and Taylor, 1976, 1977; Taylor and Forester, 1979; Gregory and Taylor, 1981; Criss and Taylor, 1986; Ferry et al., 1987; Stakes and Taylor, 1992). In these cases, the slow rates of mineralogic and isotopic alteration of clinopyroxene, combined with relatively short thermal events, led to widespread disequilibrium. Our observations thus suggest that the only portion of the study area in which isotopic equilibrium can be assumed for whole-rock–H_2O exchange is within 250 m of the contact in the pyroxene zone.

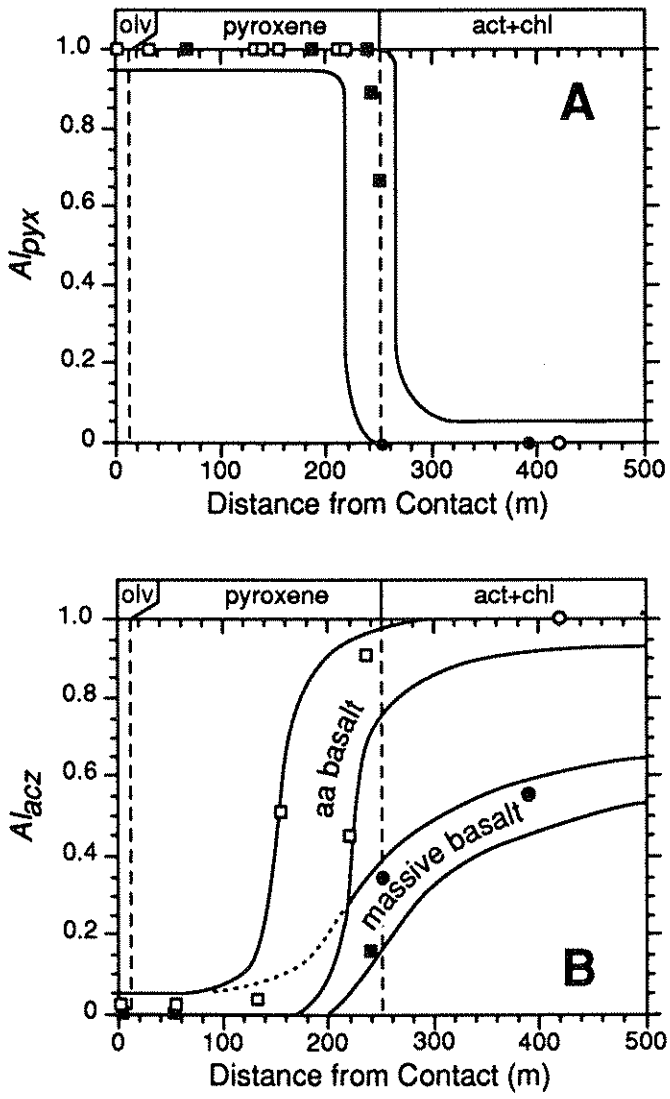

Figure 8. Variation in alteration index (AI) with distance from the contact in the pyroxene (pyx) and actinolite + chlorite (acz) zones. See Figure 6 for mineral zone abbreviations and symbols.

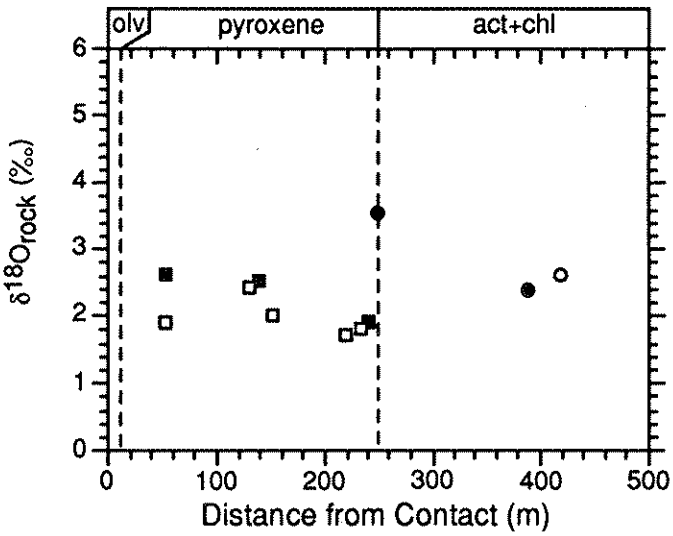

Figure 9. Variation in $\delta^{18}O_{rock}$ in aa and massive basalts with distance from the contact. See Figure 6 for mineral zone abbreviations and symbols.

DISCUSSION

Macroscopic porosity and extent of metamorphic reactions

That AI_{pyx} does not depend on lithology but AI_{acz} does (Fig. 8) suggests that the effect of porosity on basalt metamorphism is a function of temperature and the reactant and product phases. The mineral assemblage in the high-temperature pyroxene and olivine zones is dominantly anhydrous, with less than a few modal percent biotite and no hornblende. Because the basalts were largely unaltered prior to gabbro emplacement (Manning et al., 1993), the prograde reactions in these zones involved formation of an anhydrous metamorphic assemblage from an anhydrous basalt protolith. Water is neither produced nor consumed by these reactions, so factors influencing H_2O transport to or from reaction sites, such as primary porosity, should not affect the extent of prograde metamorphism. Moreover, the high temperatures of the pyroxene and olivine zone metamorphism imply relatively rapid rates of dissolution and precipitation reactions, which would also minimize the effect of porosity contrasts on the extent of metamorphism. Note that the lack of dependence of AI_{pyx} on lithology is not caused by rapid pore filling in the pyroxene and olivine zones, because sufficient contrasts in porosity re-

mained after peak conditions that the extents of retrograde alteration differ for each lithology (Fig. 8B).

Figure 8B shows that the extent of reactions involving the formation of actinolite + chlorite zone minerals is controlled by primary porosity. The dependence on porosity is most pronounced beyond ~150 m from the contact, suggesting that important contrasts in porosity persisted after peak conditions in this part of the aureole. Unlike the prograde metamorphic reactions in the pyroxene zone, the formation of mineral assemblages of the actinolite + chlorite zone from fresh basalt or from prograde metabasalt were hydration reactions that consumed H_2O. This is illustrated by a simple reaction in the model basalt system $CaO\text{-}MgO\text{-}Al_2O_3\text{-}SiO_2\text{-}H_2O$:

$$\underset{\text{pyroxene}}{(CaMgSi_2O_6 + 9MgSiO_3)} + \underset{\text{plagioclase}}{CaAl_2Si_2O_8} + 5H_2O \rightarrow \underset{\text{actinolite}}{Ca_2Mg_5Si_8O_{22}(OH)_2} + \underset{\text{chlorite}}{Mg_5Al_2Si_3O_{10}(OH)_8} + \underset{\text{quartz}}{2SiO_2}. \quad (1)$$

Because the progress of this model hydration reaction depends in part on the availability of H_2O as a reactant, the abundance, connectivity, and proximity of pores may influence the extent of development of the product assemblage. In addition, at the lower temperatures of the actinolite + chlorite zone, slower rates of reaction may act to enhance the effects of porosity contrasts.

Macroscopic porosity and fluid flow

Measured whole-rock oxygen isotope ratios are related to time-integrated fluid flux at a distance z along a flow path for a metamorphic event of duration t through

$$\delta^{18}O_{rock}(z,t) = \delta^{18}O_{rock}(z,t_0) + \delta^{18}O_{fluid}(z\text{-}B',t_0) - \delta^{18}O_{fluid}(z,t_0) \quad (2)$$

(Dipple and Ferry, 1992), where t_0 is the time of inception of metamorphism and B' is the molar time-integrated fluid flux divided by the number of moles of oxygen per cm^3 of rock for aqueous fluids such as those of the Skaergaard hydrothermal system (Taylor and Forester, 1979; Bird et al., 1986; Manning, 1989). The one-dimensional treatment of oxygen isotope transport represented by equation 2 is highly simplistic; we use it here to provide a first-order illustration of how primary porosities influenced metamorphic fluid flow in the massive and aa basalts. Manning et al. (1993) gave a more detailed analysis of heat and fluid flow at the Skaergaard's eastern contact by combining numerical simulations, phase equilibrium constraints, and the oxygen isotope data.

Equation 2 can be solved for time-integrated fluid flux assuming that exchange equilibrium existed over the history of isotopic reactions and that oxygen isotope exchange reactions occurred at a constant gradient in temperature along the flow path (Dipple and Ferry, 1992). As noted above, whole-rock oxygen isotope data probably reflect isotopic equilibrium only for the pyroxene zone, and we limit our discussion to this portion of the aureole. With respect to the assumption of a constant temperature gradient, the textures and mineral identities clearly imply that mineralogic reactions occurred during both heating and cooling of the pyroxene zone, and some consideration must be given to the possibility of isotopic exchange during both prograde and retrograde metamorphism. We therefore calculated time-integrated fluxes using model peak and retrograde temperature gradients (Fig. 10A). These temperature gradients were taken from the optimal simulation of Manning et al. (1993), in which time- and volume-averaged basalt permeability was 10^{-16} m^2. In this simulation, peak temperatures of ~700 °C in the outer pyroxene zone were attained ~10,000 yr after magma emplacement. To evaluate the effects

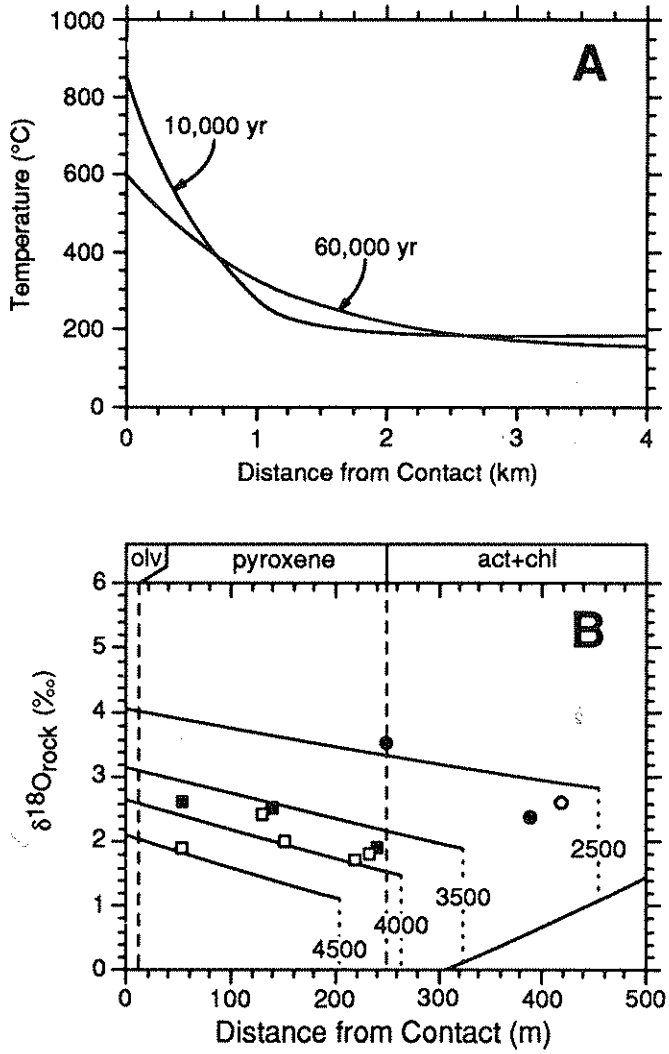

Figure 10. A: Model temperature gradients at 10,000 and 60,000 yr after emplacement of the Skaergaard magma from the simulations of Manning et al. (1993). These temperature gradients were used to compute prograde and retrograde time-integrated fluid fluxes, respectively (see text). B: Values of $\delta^{18}O_{rock}$ for aa and massive basalts vs. distance from the contact, contoured for time-integrated fluid flux 10,000 yr after magma emplacement (see text). See Figure 6 for mineral-zone abbreviations and symbols.

of isotopic exchange during cooling in the pyroxene zone, we used the temperature gradient at 60,000 yr after emplacement, when temperatures in much of the pyroxene zone were near the maximum thermal stability inferred for the actinolite + chlorite zone assemblage (~550 °C; Manning et al., 1993) and retrograde reaction rates were probably greatest.

Oxygen isotope and fluid-inclusion studies of pore-filling quartz yield $\delta^{18}O_{H_2O}$ of –0.5‰ to +0.2‰ throughout the area shown in Figure 1 (Manning, 1989), so we assumed that $\delta^{18}O_{fluid}(z,t_0) = 0.0‰$. This water composition reflects a +14‰ shift relative to Tertiary meteoric surface waters (Taylor and Forester, 1979), presumably from exchange during downward percolation through the basalt stratigraphy. Without data on the isotopic compositions of constituent minerals, basalt-water fractionation can be taken as that of plagioclase-water (e.g., Forester and Taylor, 1977). We used O'Neil and Taylor's (1967) expression for plagioclase-water exchange with $X_{An} = 0.55$ for prograde exchange and $X_{An} = 0.15$ for retrograde exchange (Fig. 6A and Table 2). We also assumed that $\delta^{18}O_{rock}(z,t_0) = 5.7‰$ (see above), that flow directions were horizontal and toward the contact (Manning and Bird, 1991), and that microscopic porosity of the analyzed rock matrices can be ignored. Finally, we assumed that local exchange equilibrium between hydrothermal fluid and secondary minerals occurred above 300 °C along the flow path (Dipple and Ferry, 1992). This is not inconsistent with our suggestion that whole-rock oxygen isotope compositions are disequilibrium values upstream of the pyroxene zone, because it requires only that the fluid equilibrates isotopically with secondary minerals. Studies comparing amphibole, pyroxene, and plagioclase isotopic compositions indicate that plagioclase and secondary amphiboles record isotopic exchange equilibrium, whereas relict igneous pyroxenes do not during alteration of basaltic bulk compositions (e.g., Stakes et al., 1984; Stakes and Taylor, 1992).

Figure 10B shows the whole-rock oxygen isotope data as a function of distance from the contact as in Figure 9, but contoured for time-integrated fluid flux computed at peak temperatures. For a constant time-integrated flux, $\delta^{18}O_{rock}$ decreases with increasing distance from the contact to a discontinuity in equation 2 at z-B', which reflects the downstream propagation of the transition from disequilibrium to local exchange equilibrium at t_0 (~800 m; Fig. 10A). Beyond the discontinuities, all flux isopleths lie on the same curve with positive slope, corresponding to complete exchange with the infiltrating fluid. Note that if the assumed temperature of equilibration were lower, the discontinuities in the flux isopleths would shift to greater distances from the contact, but the positions of the isopleths would remain the same.

Samples from the pyroxene zone suggest the flow of 3.5 to 4.5×10^3 mol cm^{-2} of aqueous fluid during prograde metamorphism. The massive samples lie within a narrow range of fluxes of 3.5 to 3.8×10^3 mol cm^{-2} with an average of 3.6×10^3 mol cm^{-2}. The aa clasts suggest similar to greater values of 3.5 to 4.5×10^3 mol cm^{-2} with an average of 4.0×10^3 mol cm^{-2}, or 10% more than the time-integrated fluxes calculated for massive samples. We interpret the lower apparent time-integrated fluid fluxes implied by the whole-rock oxygen isotope compositions in the actinolite + chlorite zone as artifacts of the lack of exchange equilibrium in this zone.

A comparison of the magnitudes of time-integrated fluid flux also must consider the retrograde alteration in the pyroxene zone. The relation between $\delta^{18}O_{rock}$ and AI_{acz} is illustrated in Figure 11A. Values of $\delta^{18}O_{rock}$ are 1.9‰ to 2.6‰ at $AI_{acz} \leq 0.05$. At higher AI_{acz}, $\delta^{18}O_{rock}$ is independent of the extent of retrograde alteration (1.9‰ ± 0.1‰). Figure 11A shows that the dependence of $\delta^{18}O_{rock}$ on the extent of retrograde alteration is ambiguous. If sample 1339-4 is ignored, the data suggest that $\delta^{18}O_{rock}$ decreases with increasing modal volume of retrograde minerals where AI_{acz}, < 0.2, but that above this value, $\delta^{18}O_{rock}$ is constant. Alternatively, is sample 1339-4 is not ignored, there is no obvious relation between $\delta^{18}O_{rock}$ and AI_{acz}. In view of the strong heterogeneities to be expected in

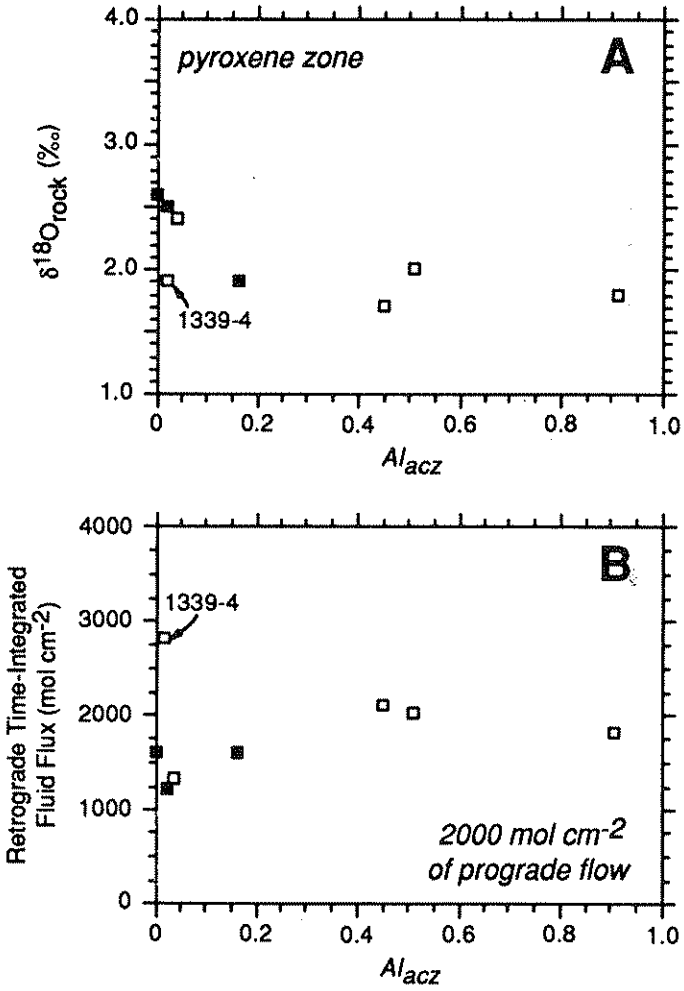

Figure 11. A: Values of $\delta^{18}O_{rock}$ for aa and massive basalts from the pyroxene zone vs. modal volume of retrograde minerals (AIa_{cz}). B: Retrograde time-integrated fluid flux vs. modal volume of retrograde minerals (AI_{acz}) in the pyroxene zone 60,000 yr after magma emplacement (see text).

the evolving pore network (Manning and Bird, 1991), there is no a priori reason to suppose that retrograde mineralogic and isotopic exchange affected each sample to the same degree. For example, the low $^{18}O/^{16}O$ at low AI_{acz} of sample 1339-4 may simply be a consequence of locally more extensive interaction with hydrothermal fluids and greater pore filling at peak conditions. Thus, some samples may record only prograde exchange, whereas others may record both prograde and retrograde exchange (cf. Fig. 8B).

To provide an end-member case for comparisons with calculations assuming only prograde flow, we assumed initial $\delta^{18}O_{rock}(z,t_0)$ values in the pyroxene zone that were predicted for a prograde flux lower than that suggested by the data in Figure 9B, but the same for both basalt morphologies (e.g., 2.0×10^3 mol cm^{-2}). We then computed retrograde time-integrated fluxes using the 60,000 yr temperature gradient (Fig. 10A). Calculated retrograde values range from 1.2 to 2.8×10^3 mol cm^{-2} (Fig. 11B) and, as when only prograde flow is assumed, aa samples record slightly higher average time-integrated fluxes than massive samples. When retrograde values are added to the assumed 2.0×10^3 mol cm^{-2} of prograde flow, the total range in time-integrated flux is 3.2 to 4.8×10^3 mol cm^{-2}, virtually identical to the values obtained assuming only prograde fluid flow. Because this observation holds independent of the magnitude of the prograde flux assumed, we conclude that the whole-rock isotopic compositions in the pyroxene zone require the flow of $\sim 4.0 \pm 0.5 \times 10^3$ mol cm^{-2} of aqueous fluid over the duration of the metamorphic event. Moreover, Figures 10 and 11 imply that units with greater macroscopic porosity record 10% higher average time-integrated molar fluxes.

The above observations are based on relatively few analyses, and the differences in $\delta^{18}O_{rock}$ are small. Numerous oxygen isotope studies of mafic contact aureoles have found that local intersample variations in $\delta^{18}O$ may exceed several parts per mil (e.g., Forester and Taylor, 1976, 1977; Andrew and O'Neil, 1988). Although a larger sample suite would probably increase the range in $\delta^{18}O_{rock}$ in our study, we emphasize that these variations should nevertheless reflect the local variations in fluid flow history. In this context, we believe that the small isotopic differences between the two lava types are meaningful, though they might be ascribed to "scatter" were porosity contrasts not explicitly recognized.

Porosity, permeability, and basalt metamorphism

Our study shows that primary porosity contrasts led to variations in mineralogic and isotopic alteration during basalt metamorphism, implying that aa and massive units had contrasting permeabilities as well. The pore morphologies also suggest higher permeabilities in the more porous units. Macroscopic pores in massive units were isolated vesicles, with little macroscopic connectivity, whereas the irregular clast interspace in aa units locally had a high degree of macroscopic connectivity (Manning and Bird, 1991).

The magnitude of any permeability differences can be evaluated using the differences in time-integrated fluid flux between the two lithologies and Darcy's Law, which states that the mass flux of fluid (u) is equal to the effective gradient in fluid pressure times the ratio of the permeability (k) to the kinematic viscosity of the fluid. The pressure gradient and kinematic viscosity can be assumed to be equal at any given point in the aureole independent of lava morphology, so differences in flux between the units can be related to differences in permeability through

$$\frac{u_{massive}}{u_{aa}} = \frac{k_{massive}}{k_{aa}} \quad (3)$$

If u is constant over time for a given time-integrated flux, which is implicit in the treatment of oxygen isotopes above, equation 3 shows that the ratio of time-integrated fluid flux is equivalent to the ratio of the time-averaged permeabilities. Thus a 10% difference in time-integrated fluid flux corresponds to a 10% difference in time-averaged permeability.

Manning et al. (1993) used numerical simulations to show that time-averaged permeabilities during metamorphism of the basalts, assuming no lithologic variation, were $\sim 10^{-16}$ m. The equal volumes of aa and massive units in the study area (Fig. 2) requires that $(\bar{k}_{massive} + \bar{k}_{aa})/2 = 10^{-16}$m^2, where $\bar{k}$ is time-averaged permeability for the subscripted lithology. Using the mean values of time-integrated prograde fluid flux and appropriate substitution into equation 3, time-averaged permeabilities were 0.95×10^{-16} m^2 for massive basalt and 1.05×10^{-16} m^2 for aa basalt. Note that independent of the accuracy of time and volume-averaged permeability inferred from numerical simulations, the ~10% difference between lithologies will still hold.

Within 1–2 km of Earth's surface, lithological differences like those between the aa and massive basalts may result in permeability contrasts of several orders of magnitude. The mean macroscopic primary porosities of aa (11%) and massive 4%) units differ by a factor of nearly three. Our study shows that these contrasts led to large local variations in the extents of reactions that produced the actinolite + chlorite zone assemblage and minor differences in $\delta^{18}O_{rock}$. However, the contrasts in time-integrated fluid flux and time- and volume-averaged permeabilities are small. Because the time-integrated fluxes derived from oxygen isotopic ratios provide a measure of the permeability of grain boundary regions, where the exchange reactions between minerals and fluid occur, our results imply that the microscopic hydrologic properties were more nearly similar than the macroscopic differences would suggest. Taken together, these conclusions show that explicit provision for differences in primary porosity gives an effective framework for understanding how basalts respond to metamorphic fluid flow on a variety of scales. Thus, the recognition of hydrologic contrasts should allow more detailed analyses of basalt metamorphism in other contact aureoles, as well as in regional terranes and subaerial and submarine hydrothermal systems.

ACKNOWLEDGMENTS

We thank John Ferry and Brooks Hanson for constructive reviews of the manuscript. The work benefited from discussions with Nick Rose, Minik Rosing, Kent Brooks, Troels Nielsen, and David Rothstein. We appreciate the assistance of D. White, of the U.S. Geological Survey, Menlo Park, California, who determined isotopic ratios. Platinova Resources, Ltd., the Geological Survey of Greenland, and the Geological Society of America provided field support. Portions of this study have been supported by National Science Foundation grants EAR-9104288 to Manning and EAR-8606256 and EAR-8802754 to Bird.

REFERENCES CITED

Anderson, D. J., Lindsley, D. H., and Davidson, P. M., 1993, QUILF: A PASCAL program to assess equilibria among Fe-Mg-Mn-Ti oxides, pyroxenes, olivine, and quartz: Computers & Geosciences, v. 19, p. 1333–1350.

Andrew, A. S., and O'Neil, J. R., 1988, Role of fluids during contact metamorphism: Stable isotope evidence from the Rockley volcanics, eastern Australia: American Journal of Science, v. 288, p. 490–511.

Atlantic-Richfield Hanford Company, 1976, Preliminary feasibility study of storage of radioactive wastes in Columbia River Basalts: Hanford, Report ARH-ST-137, v. 1, 168 p.

Bayliss, P., 1975, Nomenclature of the trioctahedral chlorites: Canadian Mineralogist, v. 13, p. 178–180.

Bence, A. E., and Albee, A. L., 1968, Empirical correction factors for the electron microanalysis of silicates and oxides: Journal of Geology, v. 76, p. 382–403.

Bird, D. K., Rosing, M. T. Manning, C. E., and Rose, N. M., 1985, Geologic field studies of the Miki Fjord area, East Greenland: Geological Society of Denmark Bulletin, v. 34, p. 219–236.

Bird, D. K., Rogers, R. D., and Manning, C. E., 1986, Mineralized fracture systems of the Skaergaard intrusion: Meddelser om Grønland, Geoscience, v. 16, 68 p.

Bird, D. K., Manning, C. E., and Rose, N. M., 1988, Hydrothermal alteration of Tertiary layered gabbros, East Greenland: American Journal of Science, v. 288, p. 405–457.

Brace, W. F., 1980, Permeability of crystalline and argillaceous rocks: Status and problems: International Journal of Rock Mechanics in Mineral Science and Geomechanical Abstracts, v. 17, p. 876–893.

Brooks, C. K., 1980, Episodic volcanism, epeirogenesis and the formation of the North Atlantic Ocean: Palaeogeography, Palaeoclimatology, Palaeoecology, v. 30, p. 229–242.

Brooks, C. K., and Gleadow, A. J. W., 1979, A fission-track age for the Skaergaard intrusion and the age of the East Greenland basalts: Geology, v. 5, p. 539–540.

Brooks, C. K., and Nielsen, T. F. D., 1982a, The Phanerozoic development of the Kangerdlugssuaq area, East Greenland: Meddelser om Grønland, Geoscience, v. 9, 30 p.

Brooks, C. K., and Nielson, T. F. D., 1982b, The East Greenland continental margin: A transition between oceanic and continental magmatism: Geological Society of London Journal, v. 139, p. 265–275.

Chamberlain, C. P., and Conrad, M. E., 1991, The relative permeabilities of quartzites and schists during active metamorphism at mid-crustal levels: Geophysical Research Letters, v. 18, p. 959–962.

Chambers, W. F., 1985, SANDIA TASK8: A subroutined electron microprobe automation system: Sandia National Laboratories Report SAND85-2037, 115 p.

Criss, R. E., and Taylor, H. P., Jr., 1986, Meteoric-hydrothermal systems, *in* Valley, J. W., Taylor, H. P., and O'Neil, J. R., eds., Stable isotopes: Mineralogical Society of America Reviews in Mineralogy, v. 16, p. 373–424.

Davis, S. N., 1969, Porosity and permeability in natural materials, *in* DeWiest, R. J. M., ed., Flow through porous media: New York, Academic Press, p. 54–89.

Dipple, G. M., and Ferry, J. M., 1992, Fluid flow and stable isotopic alteration in rocks at elevated temperatures with applications to metamorphism: Geochimica et Cosmochimica Acta, v. 56, p. 3539–3550.

Drost, B. W., Whiteman, K. J., and Gonthier, J. B., 1990, Geologic framework of the Columbia Plateau aquifer system, Washington, Oregon, and Idaho: U.S. Geological Survey Water-Resources Investigation 87-4238, 10 p.

Ferry, J. M., 1985, Hydrothermal alteration of Tertiary igneous rocks from the Isle of Skye, northwest Scotland. I. Gabbros: Contributions to Mineralogy and Petrology, v. 91, p. 264–282.

Ferry, J. M., 1986, Reaction progress: A monitor of fluid-rock interaction during metamorphism and hydrothermal events, *in* Walther, J. V., and Wood, B. J., eds., Fluid-rock interactions during metamorphism: Advances in Physical Geochemistry, v. 5, p. 60–88.

Ferry, J. M., 1988, Contrasting mechanisms of fluid flow through adjacent stratigraphic units during regional metamorphism, south-central Maine, USA: Contributions to Mineralogy and Petrology, v. 98, p. 1–12.

Ferry, J. M., Mutti, L. J., and Zuccala, G. J., 1987, Contact metamorphism/hydrothermal alteration of Tertiary basalts from the Isle of Skye, northwest Scotland: Contributions to Mineralogy and Petrology, v. 95, p. 166–181.

Forester, R. W., and Taylor, H. P., Jr., 1976, ^{18}O-depleted igneous rocks from the Tertiary complex of the Isle of Mull, Scotland: Earth and Planetary Science Letters, v. 32, p. 11–17.

Forester, R. W., and Taylor, H. P., Jr., 1977, $^{18}O/^{16}O$, D/H, and $^{13}C/^{12}C$ studies of the Tertiary igneous complex of Skye, Scotland: American Journal of Science, v. 277, p. 136–177.

Gonthier, J. B., 1990, Geology, structure, and thickness of hydrogeologic units in part of the Columbia Plateau, Oregon: U.S. Geological Survey Water-Resources Investigations 86-4001, 6 sheets.

Gregory, R. T., and Taylor, H. P., Jr., 1981, An oxygen isotope profile in a section of Cretaceous oceanic crust, Samail ophiolite, Oman: Evidence for $\delta^{18}O$ buffering of the oceans by deep (>5 km) seawater-hydrothermal circulation at mid-ocean ridges: Journal of Geophysical Research, v. 86, p. 2737–2755.

Guidotti, C. V., 1984, Micas in metamorphic rocks, *in* Bailey, S. W., ed., Micas: Mineralogical Society of America Reviews in Mineralogy, v. 13, p. 357–467.

Hirschmann, M., 1992, Origin of the transgressive granophyres from the Layered Series of the Skaergaard intrusion, East Greenland: Journal of Volcanology and Geothermal Research, v. 52, p. 185–207.

Hunt, C. D., Jr., Ewart, C. J., and Voss, C. I., 1988, Region 27, Hawaiian Islands, *in* Back, W., Rosenshein, J. S., and Seaber, P. R., eds., Hydrogeology: Boulder, Colorado, Geological Society of America, The Geology of North America, v. O-2, p. 255–262.

Ingebritsen, S. E., and Scholl, M. A., 1993, The hydrogeology of Kilauea volcano: Geothermics, v. 22, p. 255–270.

Larsen, L. M., and Watt, W. S., 1985, Episodic volcanism during break-up of the North Atlantic: Evidence from the East Greenland plateau basalts: Earth and Planetary Science Letters, v. 73, p. 105–116.

Larsen, L. M., Watt, W. S., and Watt, M., 1989, Geology and petrology of the lower Tertiary plateau basalts of the Scoresby Sund region, East Greenland: Grønlands Geologiske Undersøgelse, Bulletin 157, 164 p.

Leake, B. E., 1978, Nomenclature of amphiboles: Canadian Mineralogist, v. 16, p. 501–520.

Lindholm, G. F., and Vaccaro, J. J., 1988, Region 2, Columbia lava plateau, *in* Back, W., Rosenshein, J. S., and Seaber, P. R., eds., Hydrogeology: Boulder, Colorado, Geological Society of America, The Geology of North America, v. O-2, p. 37–50.

Liou, J. G., Maruyama, S., and Cho, M., 1985, Phase equilibria and mineral

parageneses of metabasites in low-grade metamorphism: Mineralogical Magazine, v. 49, p. 321–333.

Manning, C. E., 1989, Porosity evolution, contact metamorphism, and fluid flow in the host basalts of the Skaergaard magma-hydrothermal system [Ph.D. thesis]: Stanford, California, Stanford University, 190 p.

Manning, C. E., and Bird, D. K., 1986, Hydrothermal clinopyroxenes of the Skaergaard intrusion: Contributions to Mineralogy and Petrology, v. 92, p. 437–447.

Manning, C. E., and Bird, D. K., 1990, Fluorian garnets from the host rocks of the Skaergaard intrusion: Implications for metamorphic fluid composition: American Mineralogist, v. 75, p. 859–873.

Manning, C. E., and Bird, D. K., 1991, Porosity evolution and fluid flow in the basalts of the Skaergaard magma-hydrothermal system, East Greenland: American Journal of Science, v. 291, p. 201–257.

Manning, C. E., Ingebritsen, S. E., and Bird, D. K., 1993, Missing mineral zones in contact metamorphosed basalts: American Journal of Science, v. 293, p. 894–938.

Maruyama, S., Suzuki, K., and Liou, J. G., 1983, Greenschist-amphibolite transition equilibria at low pressures: Journal of Petrology, v. 24, p. 583–604.

Moskowitz, B., and Norton, D., 1977, A preliminary analysis of intrinsic fluid and rock resistivity in active hydrothermal systems: Journal of Geophysical Research, v. 82, p. 5787–5795.

Myers, J. S., 1978, Skaergaard intrusion, East Greenland: Contact metamorphism and deformation on Mellemö: Geological Society of Denmark Bulletin, v. 28, p. 1–4.

Nabelek, P. I., Labotka, T. C., O'Neil, J. R., and Papike, J. J., 1984, Contrasting fluid/rock interaction between the Notch Peak granitic intrusion and argillites and limestones in western Utah: Evidence from stable isotopes and phase assemblages: Contributions to Mineralogy and Petrology, v. 86, p. 25–34.

Nielsen, T. F. D., 1978, The Tertiary dike swarms of the Kangerdlugssuaq area, east Greenland. An example of magmatic development during continental break-up: Contributions to Mineralogy and Petrology, v. 67, p. 63–78.

Nielsen, T. F. D., Soper, N. J., Brooks, C. K., Faller, A. M., Higgins, A. C., and Matthews, D. W., 1981, The pre-basaltic sediments and the lower basalts at Kangerdluggssuaq, East Greenland: Their stratigraphy, lithology, palaeomagnetism and petrology: Meddelser om Grønland, Geoscience, v. 6, 25 p.

Norton, D., 1984, Theory of hydrothermal systems: Annual Review of Earth and Planetary Sciences, v. 12, p. 155–177.

Norton, D., 1988, Metasomatism and permeability: American Journal of Science, v. 288, p. 604–619.

Norton, D., 1990, Pore fluid pressure near magma chambers, *in* The role of fluids in crustal processes: Washington, D.C., National Academy Press, p. 42–49.

Norton, D., and Knapp, R., 1977, Transport phenomena in hydrothermal systems: The nature of porosity: American Journal of Science, v. 277, p. 937–981.

Norton, D., and Taylor, H. P., Jr., 1979, Quantitative simulation of the hydrothermal systems of crystallizing magmas on the basis of transport theory and oxygen isotope data: An analysis of the Skaergaard intrusion: Journal of Petrology, v. 20, p. 421–486.

Norton, D., Taylor, H. P., Jr., and Bird, D. K., 1984, The geometry and high temperature brittle deformation of the Skaergaard intrusion: Journal of Geophysical Research, v. 89, p. 10,178–10,192.

O'Neil, J. R., and Taylor, H. P., Jr., 1967, The oxygen isotope and cation exchange chemistry of feldspars: American Mineralogist, v. 52, p. 1414–1437.

Soper, N. J., Higgins, A. C., Downie, C., Matthews, D. W., and Brown, P. E., 1976a, Late Cretaceous–Tertiary stratigraphy of the Kangerdlugssuaq area, east Greenland, and the age of the opening of the north-east Atlantic: Geological Society of London Journal, v. 132, p. 85–104.

Soper, N. J., Downie, C., Higgins, A. C., and Costa, L. I., 1976b, Biostratigraphic ages of Tertiary basalts on the east Greenland continental margin and their relationship to plate separation in the northeast Atlantic: Earth and Planetary Science Letters, v. 32, p. 149–157.

Stakes, D. S., and Taylor, H. P., Jr., 1992, The northern Samail ophiolite: An oxygen isotope, microprobe, and field study: Journal of Geophysical Research, v. 97, p. 7043–7080.

Stakes, D. S., Taylor, H. P., Jr., and Fisher, R. L., 1984, Oxygen-isotope and geochemical characterization of hydrothermal alteration in ophiolite complexes and modern oceanic crust, *in* Gass, I. G., Lippard, S. J., and Shelton, A. W., eds., Ophiolites and oceanic lithosphere: Geological Society of London Special Publication 14, p. 199–214.

Stearns, H. T., 1942, Hydrology of lava-rock terranes, *in* Meinzer, O. E., ed., Hydrology: New York, McGraw-Hill, p. 678–703.

Stearns, H. T., and Vaksvik, K. N., 1935, Geology and ground-water resources of the island of Oahu: Hawaii Division of Hydrography Bulletin 1, 479 p.

Takasaki, K. J., and Valenciano, S., 1969, Water in the Kahuku area, Oahu, Hawaii: U.S. Geological Survey Water-Supply Paper 1778, 133 p.

Taylor, H. P., Jr., and Forester, R. W., 1979, An oxygen isotope study of the Skaergaard intrusion and its country rocks: A description of a 55-m.y. old fossil hydrothermal system: Journal of Petrology, v. 20, p. 355–419.

Taylor, H. P., Jr., and Sheppard, 1986, Igneous rocks: I. Processes of isotopic fractionation and isotope systematics, *in* Valley, J. W., Taylor, H. P., and O'Neil, J. R., eds., Stable isotopes: Mineralogical Society of America Reviews in Mineralogy, v. 16, p. 227–271.

Titley, S. R., 1990, Evolution and style of fracture permeability in intrusion-centered hydrothermal systems, *in* The role of fluids in crustal processes: Washington, D.C., National Academy Press, p. 50–63.

Uhl, V. W., and Joshi, V. G., 1986, Results of pumping tests in the Deccan Trap basalts of central India: Journal of Hydrology, v. 86, p. 147–168.

Wager, L. R., and Brown, G. M., 1967, Layered igneous rocks: San Francisco, W. H. Freeman, 588 p.

Wager, L. R., and Deer, W. A., 1939, Geological investigations in East Greenland. III. The petrology of the Skaergaard intrusion, Kangerdlugssuaq, East Greenland: Meddeleser om Grønland, v. 105, 352 p.

Walder, J., and Nur, A., 1984, Porosity reduction and crustal pore pressure development: Journal of Geophysical Research, v. 89, p. 11,539–11,548.

Walker, G. P. L., 1960, Zeolite zones and dike distribution in relation to the structure of the basalts of eastern Iceland: Journal of Geology, v. 68, p. 515–528.

Wood, W. W., and Fernandez, L. A., 1988, Volcanic rocks, *in* Back, W., Rosenshein, J. S., and Seaber, P. R., eds., Hydrogeology: Boulder, Colorado, Geological Society of America, The Geology of North America, v. O-2, p. 353–365.

MANUSCRIPT ACCEPTED BY THE SOCIETY MARCH 25, 1994

Printed in U.S.A.